

Radiative feedback from high mass X-ray binaries on the formation of the first galaxies and early reionization

Myoungwon Jeon^{1*}, Andreas H. Pawlik², Volker Bromm¹, Miloš Milosavljević¹

¹*Department of Astronomy and Texas Cosmology Center, University of Texas, Austin, TX 78712, USA*

²*Max-Planck-Institut für Astrophysik, Karl-Schwarzschild-Strasse 1, 85748 Garching bei München, Germany*

ABSTRACT

Recent work suggests that the first generation of stars, the so-called Population III (Pop III), could have formed primarily in binaries or as members of small multiple systems. Here we investigate the impact of X-ray feedback from High-Mass X-ray Binaries (HMXBs) left behind in stellar binary systems after the primary forms a black hole (BH), accreting gas at a high rate from the companion, a process that is thought to be favored at the low metallicities characteristic of high-redshift gas. Thanks to their large mean free path, X-rays are capable of preionizing and preheating the gas in the intergalactic medium (IGM) and in haloes long before the reionization of the Universe is complete, and thus could have strongly affected the formation of subsequent generations of stars as well as reionization. We have carried out zoomed hydrodynamical cosmological simulations of minihaloes, accounting for the formation of Pop III stars and their collapse into BHs and HMXBs, and the associated radiation-hydrodynamic feedback from UV and X-ray photons. We find no strong net feedback from HMXBs on the simulated star formation history. On the other hand, the preheating of the IGM by HMXBs leads to a strong suppression of small-scale structures and significantly lowers the recombination rate in the IGM, thus yielding a net positive feedback on reionization. We further show that X-ray feedback from HMXBs can augment the ionizing feedback from the Pop III progenitor stars to suppress gas accretion onto the first BHs, limiting their growth into supermassive BHs. Finally, we show that X-ray ionization by HMXBs leaves distinct signatures in the properties of the high-redshift hydrogen that may be probed in upcoming observations of the redshifted 21 cm spin-flip line.

Key words: cosmology: observations – galaxies: formation – galaxies: high-redshift – HII regions – hydrodynamics – intergalactic medium – black holes: physics.

1 INTRODUCTION

A key question in modern cosmology is to understand how the cosmic dark ages ended with the emergence of the first sources of light (Loeb 2010; Wiklind et al. 2013). The nature of this transition is largely driven by the properties of the first stars, also known as Population III (Pop III). Recent studies of their formation, based on high-resolution simulations with realistic cosmological initial conditions, have led to an important revision in our understanding (e.g. Turk et al. 2009; Stacy et al. 2010, 2012; Clark et al. 2011; Greif et al. 2011; Prieto et al. 2011; Smith et al. 2011; Greif et al. 2012; Dopcke et al. 2013). Whereas the previous standard model had posited that the first stars formed as very massive, single stars in the centres of dark matter minihaloes

(Bromm & Larson 2004), in the revised model they typically emerge as members of small multiple systems with a range of masses (Bromm 2013).

Although the characteristic mass of the first stars is now predicted to be smaller than previously thought, of order a few $10 M_{\odot}$ instead of $\sim 100 M_{\odot}$, the initial stellar mass function (IMF) is found to be sufficiently broad that stellar masses can still reach the high values for which black hole (BH) remnants are expected to form. This is due to the ability to continuously accrete from a protostellar disk even in the presence of protostellar radiation (e.g. Hosokawa et al. 2011; Stacy et al. 2012; Hirano et al. 2013). These results open the possibility of Pop III high-mass X-ray binaries (HMXBs), where one component is a BH remnant accreting material from a companion (e.g. Mirabel et al. 2011; Haiman 2011; Xu et al. 2013).

Whether suitable Pop III binary systems can form is still quite uncertain (e.g. Saigo et al. 2004; Machida et al.

* E-mail: myjeon@astro.as.utexas.edu

2008; Power et al. 2009; Stacy & Bromm 2013). The main challenge is to extend the simulations over the entire accretion phase to ascertain whether the protostars merge or are ejected by close encounters with other protostars from the natal disk. Considering ten different minihaloes for 5000 yr, recent work by Stacy & Bromm (2013) found a binary fraction of $\sim 35\%$ and a distribution of semi-major axes that peaks at ~ 300 AU. Depending on the physical properties of binaries, those could be progenitors of gamma-ray bursts (e.g. Bromm & Loeb 2006; Belczynski et al. 2007), or sources of gravitational waves (e.g. Belczynski et al. 2004; Kowalska et al. 2012), possibly detectable by current and future gravitational wave interferometers.

In the local Universe, the dominant X-ray contribution from star-forming galaxies comes from HMXBs and ultra-luminous X-ray sources (ULXs) (e.g., Mineo et al. 2012). HMXBs and ULXs are defined by their X-ray luminosities as $L_X > 10^{36}$ erg s $^{-1}$ and $L_X > 10^{39}$ erg s $^{-1}$, respectively. Studies of the HMXB population and its dependence on metallicity, showing that low metallicity favors HMXB formation (e.g. Majid et al. 2004; Dray 2006; Soria 2007; Mapelli et al. 2009; Linden et al. 2010), support the importance of HMXBs at high redshift when the Universe was chemically pristine. This dependence on metallicity arises in part because in low-metallicity environments stellar mass-loss via radiatively-driven winds is significantly reduced (Kudritzki & Puls 2000), leading to higher BH remnant masses (Eldridge & Vink 2006; Belczynski et al. 2010). However, independent of the preference for a higher BH mass at low metallicity, the work by Linden et al. (2010), employing binary population synthesis calculations, suggests that metallicity determines the number of systems undergoing stable mass transfer via Roche lobe overflow (RLO). This implies that the parameter space of allowed stable common-envelope pathways for RLO is much wider at low than at high metallicity.

The role of radiative feedback by an isolated accreting BH left behind by a Pop III star, a so-called miniquasar, has been explored by a number of authors. Some of them focused on a single source, not including any later generations of BHs (see, e.g., Glover & Brand 2003; Kuhlen & Madau 2005; Milosavljević et al. 2009; Milosavljević et al. 2009; Alvarez et al. 2009; Park & Ricotti 2011; Venkatesan & Benson 2011; Wheeler & Johnson 2011; Jeon et al. 2012; Aykutaalp et al. 2013), or semi-analytically on the collective impact of X-rays from BHs at high redshifts (e.g. Justham & Schawinski 2012; Tanaka et al. 2012; Power et al. 2013). Given that X-rays can penetrate further than stellar ionizing photons, their impact can extend to the distant IGM. In general, X-ray heating may be expected to provide a strong negative feedback on gas collapse and star formation especially near X-ray sources. On the other hand, the efficiency of the formation of molecular hydrogen (H $_2$) and hydrogen deuteride (HD) and hence molecular cooling may be increased especially in distant collapsed structures due to the enhancement in the electron fraction by X-ray ionizations, resulting in a positive feedback on star formation in regions not too close to X-ray sources. Such dependence on distance from a source, however, might be washed out as the number of X-ray sources increases with time. Thus, we need to study the collective effect to better understand if the X-ray feedback on star formation has a positive or negative outcome.

The early establishment of an X-ray background is expected to play an important role in reionization. X-ray pre-heating might increase the cosmological Jeans, or filtering, mass. More time would then be required to form haloes more massive than the Jeans mass, thus delaying the process of reionization (see, e.g. Madau et al. 2004; Ricotti & Ostriker 2004; Holley-Bockelmann et al. 2012; Mesinger et al. 2013). On the other hand, X-ray heating might reduce small-scale structure, lowering the number of recombinations, thus in turn accelerating reionization (e.g. Haiman et al. 2001; Wise & Abel 2005, 2008a; Pawlik et al. 2009; Finlator et al. 2012; Emberson et al. 2013). The net effect is difficult to predict short of treating it with full cosmological simulations. Additionally, pre-ionization by X-rays may help explain the relatively large value of the optical depth to reionization measured by the WMAP and Planck satellites (e.g., Ricotti & Ostriker 2004; Ahn et al. 2012).

In our preceding paper (Jeon et al. 2012), we focused on investigating the formation of stars and the assembly of the first galaxies under the radiative feedback from a single isolated accreting BH and from a single HMXB, both remnants of a Pop III star. We found that with a single accreting BH whose radiative luminosity scales with the rate of accretion of diffuse halo gas, the gas within the halo hosting the BH can be photoheated up to $\sim 10^3 - 10^4$ K, preventing any subsequent star formation for a few 100 Myr inside the halo. Distant star formation outside the host halo, on the other hand, was promoted by the enhanced formation of H $_2$, which is catalyzed by the enhanced free electron fraction generated in photoionizations by the X-rays. The net positive feedback on star formation was however very mild due to competition between the positive and negative feedback, in agreement with earlier investigations (Machacek et al. 2003; Kuhlen & Madau 2005).

A stronger effect occurred in the presence of an HMXB. This was due to the stronger X-ray emission, near the Eddington limit independent of the conditions in the surrounding interstellar gas, which photoevaporated the gas and prevented gas infall into the halo center, thus establishing a stronger negative feedback inside the host system. But also the positive feedback effect was found to be stronger, yielding a net increase in the cosmological star formation rate. The radiation from the HMXB, however, was continuous for 150 Myr, unrealistically long compared to inferred HMXB lifetimes in the local Universe, which is on the order of 1 – 3 Myr (Belczynski et al. 2012; Justham & Schawinski 2012). Such an episodic HMXB irradiation might result in a much weaker effect.

In this work, we study the radiative feedback from a population of HMXBs, both locally on the gas in the host halo and globally on the IGM, using a physically motivated model for HMXBs, and improved methods to track the accretion of gas and the transport of photons in the UV and X-ray bands. Computing radiative transfer (RT) of X-ray photons is particularly challenging due to the large penetrating power of X-rays that renders each point in space visible to many sources. The TRAPHIC code (Pawlik & Schaye 2008, 2011), however, allows us to track the radiation from multiple sources, Pop III stars and HMXBs, at a computational cost that is independent of the number of sources. To the best of our knowledge, this is the first simulation

where the fully coupled radiation-hydrodynamics with multiple HMXB sources is taken into account.

This paper is organized as follows. In Section 2, we describe our simulation methods. In Section 3, we present the results of our simulations. We investigate the impact of HMXBs on the properties of the gas in the IGM and in haloes and discuss the implications for reionization and black hole growth. In Section 4, we estimate the 21 cm signal of the high-redshift gas and discuss observational constraints that can be derived from the 21 cm signal on the nature of the first ionizing sources. Finally, in Section 5, we summarize our results. Distances are expressed in physical (i.e., not comoving) units unless noted otherwise. We will make use of the species number density fractions with respect to hydrogen $\eta_\alpha \equiv n_\alpha/n_{\text{H}}$, where α labels the chemical species.

2 NUMERICAL METHODOLOGY

We have carried out cosmological Smoothed Particle Hydrodynamics (SPH) simulations of the formation of high-redshift minihaloes, following the chemistry and cooling of the primordial gas, the formation of Pop III stars and their collapse into BHs, and the ionization and photodissociation by the radiation emitted by the stars and accreting BHs.

To investigate the feedback by HMXBs we compare two simulations, which are identical except that in one of them the formation of HMXBs is suppressed, and the BHs left behind after the death of the Pop III stars are powered solely by accretion of diffuse halo gas.

In Jeon et al. (2012) we carried out a similar set of simulations of feedback from Pop III stars, accreting BHs and HMXBs. The current work improves on our previous work in several key aspects. Our simulations are run with an updated version of the SPH code GADGET (last described in Springel 2005), and we employ an improved implementation of accretion of gas by BHs and a physically motivated model of HMXBs. The ionizing radiation emitted by Pop III stars, BHs and HMXBs is followed using multi-frequency RT, and the spectrum of the radiation emerging from BHs and HMXBs includes a soft thermal contribution from the accretion disk in addition to a power-law high energy tail. Secondary ionization is accounted for depending on the energies of the primary photo-electrons. Finally, we track the photodissociation of H₂ and HD by LW photons both from the Pop III stars and the accreting BHs, taking into account local shielding in the gas. In the following, we provide a detailed description of our simulations, and refer to our preceding work where appropriate.

2.1 Gravity, hydrodynamics, and chemistry

We use the N -body/TreePM SPH code GADGET (Springel 2005; Springel et al. 2001; our specific implementation is derived from that discussed in Schaye et al. 2010). Our simulations are initialized using a snapshot from the earlier zoomed simulation of Greif et al. (2010), which was initialized at $z = 99$ in a periodic box of linear size 1 comoving Mpc, using Λ CDM cosmological parameters and matter density $\Omega_{\text{m}} = 1 - \Omega_{\Lambda} = 0.3$, baryon density $\Omega_{\text{b}} = 0.04$, present-day Hubble expansion rate $H_0 = 70 \text{ km s}^{-1} \text{ Mpc}^{-1}$, spectral index $n_{\text{s}} = 1.0$, and normalization $\sigma_8 = 0.9$, which is higher

than the value measured by the WMAP and Planck satellites (e.g., Komatsu et al. 2011; Planck Collaboration 2013). The choice of a high value of σ_8 might accelerate structure formation in our simulations. However, in this paper, we focus on the effects of radiative feedback by comparing individual haloes, and this comparison is insensitive to the variation in the σ_8 parameter. Employing consecutive levels of refinement, the masses of dark matter (DM) and SPH particles in the highest resolution region with an approximate extent of 300 comoving kpc are $m_{\text{DM}} \approx 33 M_{\odot}$ and $m_{\text{SPH}} \approx 5 M_{\odot}$, respectively.

We start the simulations at $z \approx 30$, corresponding to the time just before the first Pop III star is formed, and terminate them at $z \approx 18$. We adopt a Plummer-equivalent gravitational softening length $\epsilon_{\text{soft}} = 70$ comoving pc for both dark matter and baryonic particles. SPH quantities are estimated by averaging inside a sphere containing $N_{\text{ngb}} = 48$ neighbors and adopting the entropy conserving formulation of SPH (Springel & Hernquist 2002). The SPH kernel, i.e., the radius of this sphere, is prevented from falling below $10^{-3} \epsilon_{\text{soft}}$. The gas particle mass defines a baryonic mass resolution $M_{\text{res}} \equiv N_{\text{ngb}} m_{\text{SPH}} \approx 240 M_{\odot}$. The Jeans mass in primordial gas, in which molecular hydrogen cooling imprints a condition for primary star formation with a characteristic density of $n_{\text{H}} \simeq 10^4 \text{ cm}^{-3}$ and a temperature of $\sim 200 \text{ K}$ (Abel et al. 2000; Bromm et al. 2002), is thus marginally resolved, and the Bate & Burkert (1997) criterion to avoid artificial fragmentation is marginally satisfied.

We use the same primordial chemistry and cooling network as in Greif et al. (2010), where all relevant cooling mechanisms, i.e., by H and He collisional ionization, excitation and recombination cooling, bremsstrahlung, inverse Compton cooling, and collisional excitation cooling of H₂ and HD, are taken into account. The radiative cooling by H₂ is computed accounting for collisional excitations by protons and electrons, which is important in gas with a significant fractional ionization (Glover & Abel 2008). The code self-consistently solves the rate equations for the abundances of H, H⁺, H⁻, H₂, H₂⁺, He, He⁺, He⁺⁺, and e⁻, as well as for the three deuterium species D, D⁺, and HD, taking into account photoionization, secondary ionization, and photodissociation as described below. We set the hydrogen mass fraction to $X = 0.76$.

2.2 Sink particles

Upon reaching hydrogen number densities $n_{\text{H,max}} = 10^4 \text{ cm}^{-3}$, gas particles are converted into collisionless sink particles. Each newly formed sink particle accretes a random subset of the $N_{\text{ngb}} = 48$ neighboring gas particles residing in the SPH smoothing kernel, which defines the effective accretion radius, r_{acc} , of the progenitor gas particle, until its mass has exceeded $100 M_{\odot}$. The initial mass of sinks is thus $M_{\text{sink}} \approx 100 M_{\odot}$, which is appropriate given the adopted star formation model that we describe below.

Sink particles can grow in mass by accreting gas inside the sphere with radius r_{acc} . Sink particles that approach each other on scales below 1 pc, which is similar to the baryonic resolution scale $l_{\text{res}} \equiv [(3X M_{\text{res}})/(4\pi n_{\text{H,max}} m_{\text{H}})]^{1/3} \approx 0.5 \text{ pc}$, are merged. The position and velocity of the sink particle resulting from the merger are set to the mass-weighted

average position and velocity of the sink particles before merging.

In the following, we identify the sink particles with the sites of Pop III star formation.

2.3 Pop III binaries

Our goal is to investigate the feedback from HMXBs which may follow the formation of stellar binaries. We therefore assume for simplicity, but consistent with recent work on fragmentation of primordial gas (e.g., Turk et al. 2009; Stacy et al. 2010, 2012; Clark et al. 2011; Greif et al. 2011; Prieto et al. 2011; Smith et al. 2011; Greif et al. 2012; Dopcke et al. 2013), that all Pop III stars form in binaries. Fragmentation and the formation of binaries are treated using a sub-resolution model, assuming each sink is host to a Pop III binary system. To limit the instantaneous binary formation rate to one system per minihalo, we prevent the creation of additional sink particles for $t_{\text{sh}} = 1$ Myr in spheres with radius $r_{\text{sh}} = 30$ pc centred on each newly created sink particle. This corresponds to the time needed for photoheating by a Pop III star in a minihalo to suppress the gas density inside the spheres, assuming the resulting hydrodynamic shock propagates at $v_{\text{sh}} \approx 30 \text{ km s}^{-1}$ (e.g., Shu et al. 2002; Whalen et al. 2004; Alvarez et al. 2006).

In practice, the adopted recipe guarantees there can be at most a single active Pop III binary per minihalo at any given time. The properties of the binary system are assigned assuming that the primary dominates the mass of the system. Thus, the stellar properties of the binary are set to that of an isolated Pop III star of mass $100 M_{\odot}$. Such a star shines for 2.7 Myr emitting a black body spectrum with temperature $T_{\text{BB}} = 10^5$ K, and has a hydrogen-ionizing photon luminosity of $9.14 \times 10^{49} \text{ s}^{-1}$ and a photodissociating luminosity of $1.1 \times 10^{49} \text{ s}^{-1}$ in the LW band (e.g., Bromm et al. 2001; Schaerer 2003).

2.4 Black hole miniquasars

The fate of Pop III stars is determined by their initial masses (Heger et al. 2003). Here, we assume that the more massive Pop III companion in each binary system collapses into a BH with mass $100 M_{\odot}$. Recent studies, in which the effects of rotation of Pop III stars is taken into account, have suggested that stars with masses $\gtrsim 60 - 240 M_{\odot}$ may explode as pair instability supernovae without leaving a BH behind (e.g., Chatzopoulos & Wheeler 2012, Yoon et al. 2012). However, our conclusions are not sensitive to the adopted initial mass of the BHs.

The BH then grows by accretion of the surrounding baryons at a rate (Bondi & Hoyle 1944)

$$\dot{M}_{\text{acc}} = \frac{4\pi G^2 M_{\text{BH}}^2 \rho}{(c_s^2 + v_{\text{rel}}^2)^{3/2}}, \quad (1)$$

where c_s is the sound speed, ρ the gas density, and v_{rel} the velocity of the BH relative to the gas. We assume that a fraction $\epsilon = 0.1$ of the accreted mass is converted into ionizing radiation, as is appropriate for radiatively efficient accretion onto a Schwarzschild BH (Shakura & Sunyaev 1973). The BH thus grows in mass according to $\dot{M}_{\text{BH}} = (1 - \epsilon)\dot{M}_{\text{acc}}$. If the black hole is accreting at a high rate, it is referred to as a miniquasar (e.g., Kuhlen & Madau 2005).

The density, sound speed and relative velocity needed to evaluate the accretion rate are estimated by averaging the properties of the gas particles inside the sphere with radius r_{acc} centred on the sink particle hosting the BH, consistent with the SPH formulation. For reference, the Bondi-Hoyle radius is (e.g., Edgar 2004) $r_{\text{Bondi}} \equiv \mu m_{\text{H}} G M_{\text{BH}} / (k_{\text{B}} T) \approx 0.6 \text{ pc} (\mu/1.2) (M_{\text{BH}}/100 M_{\odot}) / (T/100 \text{ K})$, where μ is the mean molecular weight.

The mass of the sink particle M_{sink} hosting the BH closely tracks the mass M_{BH} of the BH. We achieve this by letting the sink particles swallow neighboring gas particles, randomly chosen inside the sphere with radius r_{acc} , as long as the condition $M_{\text{BH}} - M_{\text{sink}} > m_{\text{SPH}}$ is satisfied (e.g., Springel et al. 2005; Di Matteo et al. 2005; Sijacki et al. 2007; Booth & Schaye 2009). This improves our implementation of BH growth in Jeon et al. (2012), in which the BHs and sink particles grew independently.

We compute the ionizing luminosities of BHs accreting diffuse gas by normalizing the total luminosity according to

$$L_{\text{BH}} \equiv \int_0^{10 \text{ keV} / h_{\text{P}}} L_{\nu} d\nu = \frac{\epsilon}{1 - \epsilon} \dot{M}_{\text{BH}} c^2 \quad (2)$$

$$= 6.4 \times 10^{37} \text{ erg s}^{-1} \frac{\dot{M}_{\text{BH}}}{10^{-8} M_{\odot} \text{ yr}^{-1}}, \quad (3)$$

where h_{P} is Planck's constant. We further assume that the spectral energy distribution of the emerging radiation is that of a thermal multi-color disk (MCD) at frequencies lower than $\nu_{\text{NT}} \equiv 0.2 \text{ keV} / h_{\text{P}}$, and that of a non-thermal power-law component at higher frequencies, consistent with observations at low redshifts (see Figure 1 in Jeon et al. 2012; e.g., Mitsuda et al. 1984; Miller et al. 2003; Madau et al. 2004; Kuhlen & Madau 2005).

The spectrum of the radiation emitted by the multi-color disk with gas temperature profile $T = T_{\text{in}}(r/r_{\text{in}})^{-p}$, where r is the distance between the BH and the location inside the disk at which the radiation emerges and r_{in} is the inner disk radius, is (e.g., Pringle 1981; Mitsuda et al. 1984)

$$J_{\text{MCD}}(\nu) \propto \left(\frac{k_{\text{B}} T_{\text{in}}}{h_{\text{P}} \nu} \right)^{2/p} \nu^3 \int_{x_{\text{in}}}^{x_{\text{out}}} dx \frac{x^{2/p-1}}{e^x - 1}, \quad (4)$$

where T_{in} is the gas temperature at $r = r_{\text{in}}$, $x_{\text{in}} = h_{\text{P}} \nu / (k_{\text{B}} T_{\text{in}})$, and $x_{\text{out}} = h_{\text{P}} \nu / (k_{\text{B}} T_{\text{in}}) (r_{\text{out}}/r_{\text{in}})^p$. The inner radius r_{in} is set to the radius of the last stable Keplerian orbit around the BH, which for non-rotating BHs is $r_{\text{in}} = 3r_{\text{s}}$, where $r_{\text{s}} = 2GM_{\text{BH}}/c^2$ is the Schwarzschild radius, and the outer radius is set to $r_{\text{out}} = 10^4 r_{\text{in}}$. We adopt $p = 3/4$, appropriate for viscous standard disks (Shakura & Sunyaev 1973; Pringle 1981; Mitsuda et al. 1984; Kato et al. 1998) and set $T_{\text{in}} = [3GM_{\text{BH}}\dot{M}_{\text{acc}} / (8\pi\sigma_{\text{SB}}r_{\text{in}}^3)]^{1/4}$ (e.g., Pringle 1981; Kato et al. 1998), where σ_{SB} is the Stefan-Boltzmann constant.

The radiation spectrum of the power-law component is

$$J_{\text{NT}}(\nu) \propto \left(\frac{\nu}{\nu_{\text{NT}}} \right)^{-\beta}, \quad (5)$$

where we set $\beta = 1$ (e.g., Kuhlen & Madau 2005). Each of the components of the two-component spectrum is normalized by assuming that a half of the total luminosity emerges from each of the MCD and the power law component (e.g., Kuhlen & Madau 2005).

The two-component spectrum implies an ionizing lumi-

nosity in the range 13.6 eV – 10 keV of $3.1 \times 10^{35} - 3.1 \times 10^{39}$ erg s⁻¹ for a BH with mass 100 M_⊙ accreting gas at rates 10⁻¹⁰ – 10⁻⁶ M_⊙ yr⁻¹. We also compute the luminosity of the accreting BH in the LW bands by integrating the spectrum over the range of energies 11.2 – 13.6 eV. The LW luminosities of a BH with mass 100 M_⊙ accreting gas at rates encountered in our simulations 10⁻¹⁰ – 10⁻⁶ M_⊙ yr⁻¹ are $2.3 \times 10^{33} - 9.6 \times 10^{36}$ erg s⁻¹.

2.5 High-mass X-ray binaries

In one of the two simulations presented here, for a subset of the relic BHs, the primary accretes gas for a brief time directly from the low-mass stellar companion, giving rise to a HMXB.

The fraction of high-redshift stellar binaries evolving into HMXBs is uncertain. Power et al. (2009) investigated the contribution of the HMXB population in globular clusters to the high-redshift X-ray background. They used Monte Carlo models of globular clusters containing 10⁶ stars and exploring a range of stellar IMFs and initial binary orbital parameters. They found that, assuming a Kroupa (2001) IMF, up to 30 per cent of the initial binary systems may avoid dissociation after the primary star undergoes a supernova explosion, thus possibly leading to an HMXB.

Motivated by the results of Power et al. (2009), we select every third binary to evolve into an HMXB immediately after the primary turned into a BH with mass 100 M_⊙. We adopt a duration of the HMXB phase of 2 Myr, approximately corresponding to the remaining main sequence lifetime of the donor star from which the BH accretes, consistent with local observations (e.g., Belczynski et al. 2012). We assume that the HMXB has a luminosity equal to the Eddington luminosity, i.e.,

$$L_{\text{HMXB}} \equiv \int_0^{10\text{keV}/h_P} L_\nu d\nu = L_{\text{Edd}} \quad (6)$$

$$= 1.4 \times 10^{40} \text{erg s}^{-1} \left(\frac{M_{\text{BH}}}{100 M_\odot} \right), \quad (7)$$

corresponding to accretion of gas from the companion at a rate 2.2×10^{-6} M_⊙ yr⁻¹ ($M_{\text{BH}}/100M_\odot$) and a total accreted mass at the end of the HMXB phase of about $4.4M_\odot$. The adopted accretion luminosity is consistent with the inferred luminosities of ULXs in local surveys (e.g., Grimm et al. 2003). We employ the two-component spectrum of the previous section used to describe the emission of radiation by BHs accreting diffuse halo gas. Hence, assuming accretion at the Eddington rate and a BH mass of 100M_⊙, the ionizing photon luminosity of a HMXB is 3.3×10^{49} s⁻¹, and its LW luminosity is 4.7×10^{47} s⁻¹. The role of the donor star is limited to fueling the accreting BH, i.e., we ignore effects of its evolution, such as the emission of ionizing radiation or the explosion in a SN.

2.6 Hydrogen and helium ionizing radiative transfer and X-ray secondary ionization

We use the RT code TRAPHIC to transport ionizing photons (Pawlik & Schaye 2008, 2011). TRAPHIC solves the time-dependent RT equation in SPH simulations by tracing photon packets emitted by source particles through the

simulation box in a photon-conserving manner. The photon packets are transported directly on the spatially adaptive set of SPH particles and hence the RT exploits the full dynamic range of the hydrodynamical simulations. A directed transport of the photon packets radially away from the sources is accomplished despite the irregular distribution of SPH particles by guiding the photon packets inside cones. A photon packet merging technique renders the computational cost of the RT independent of the number of radiation sources. In the following, we provide a brief overview of TRAPHIC in order to motivate the meaning of the numerical parameters of the RT specified below. The reader is referred to the descriptions in Pawlik & Schaye (2008), Pawlik & Schaye (2011) and Pawlik et al. (2013) for details. The specific version employed here is identical to that used in Pawlik et al. (2013), except for the treatment of secondary ionization, which is included only here and described below.

2.6.1 Basic principles

The transport of radiation starts with the emission of photon packets by source particles (here, sinks) in N_{EC} tessellating *emission cones*. The photons in each photon packet are distributed among the subset of the $\tilde{N}_{\text{ngb}} \lesssim N_{\text{ngb}}$ neighboring SPH particles residing in the cones. In cones containing zero neighbors, an additional, so-called virtual particle is inserted to which the photon packet is then assigned. Sources emit photons using emission time steps Δt_{em} , in between which the orientation of the cones is randomly rotated to increase the sampling of the volume with photons. The spectrum of the emitted radiation is discretized using N_ν frequency bins. Each photon packet carries photons from one of these bins; therefore the number of photon packets emitted per emission time step is $N_\nu \times N_{\text{EC}}$.

The newly emitted photons are assigned a propagation direction parallel to the central axis of the associated emission cone, and, together with any other photons already present in the simulation box, are then propagated further to the *downstream* neighbors of the SPH particle at which they reside. A particle is a downstream neighbor if it is among the \tilde{N}_{ngb} neighboring gas particles and resides in the regular *transmission cone* centred on the propagation direction and subtending a solid angle of $4\pi/N_{\text{TC}}$. The parameter N_{TC} hence defines the angular resolution of the RT. If there is no downstream neighbor inside a transmission cone, like for emission, a virtual particle is created to which the photons are then propagated. The transmission cones confine the propagation of photons to the solid angle in which they were originally emitted. The transport of photons, which occurs at the user-specified speed \tilde{c} , is discretized using RT time steps Δt_r .

A given SPH particle can receive multiple photon packets within the same RT time step Δt_r . These photon packets are grouped according to their propagation directions using a set of N_{RC} tessellating *reception cones*. Photon packets whose propagation directions fall in the same reception cone are merged and replaced by a single new photon packet. Each reception cone subtends a solid angle $4\pi/N_{\text{RC}}$, and hence the parameter N_{RC} determines the angular resolution of the merging. The merging limits the maximum number of photon packets in the simulation box to $N_{\text{RC}} \times N_\nu \times N_{\text{SPH}}$,

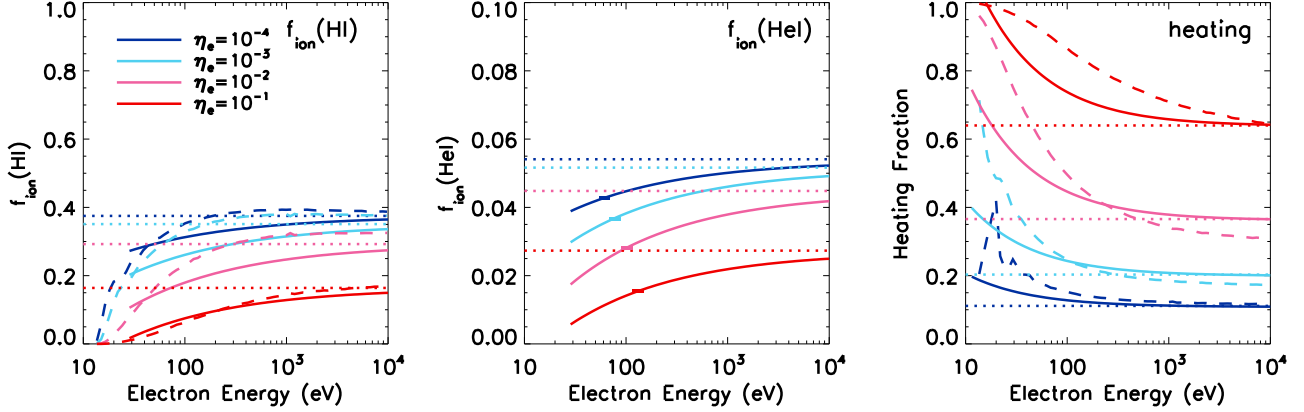


Figure 1. Fraction of the energy of the primary electron that is used in HI secondary ionization (left panel), HeI secondary ionization (middle panel) and heating (right panel). Different colors show these fractions assuming different electron fractions. The solid curves show the fits from Ricotti et al. (2002) used in the current work. The dashed curves show the more recent fits by Furlanetto & Stoever (2010) for comparison. The horizontal dotted lines show the high-energy limits from Shull & van Steenberg (1985), which we adopted independent of energy in Jeon et al. (2012). The short bars in the middle panel indicate the energies of photons with mean free path equal to the physical size of the high-resolution region of comoving extent 300 kpc in which we follow the transfer of ionizing radiation from $z = 30 - 18$.

where N_{SPH} is the number of SPH particles, and renders the computation time independent of the number of sources.

Photons are absorbed as they propagate through the gas from SPH particles to their neighbors depending on the optical depth between the two neighboring particles, respecting photon conservation (Abel et al. 1999; Mellema et al. 2006). The absorption of photons within each frequency bin is treated in the grey approximation using photoionization cross sections

$$\langle \sigma_{\alpha} \rangle_{\nu} \equiv \int_{\nu_1}^{\nu_h} d\nu \frac{4\pi J_{\nu}(\nu)}{h_{\text{P}}\nu} \sigma_{\alpha}(\nu) \times \left[\int_{\nu_1}^{\nu_h} d\nu \frac{4\pi J_{\nu}(\nu)}{h_{\text{P}}\nu} \right]^{-1}, \quad (8)$$

where $\alpha \in \{\text{HI}, \text{HeI}, \text{HeII}\}$, $J_{\nu}(\nu)$ is the spectrum, and ν_1 and ν_h are the low and high energy limits of frequency bin¹ ν . The number of absorbed photons determines the photoionization rate $\Gamma_{\gamma\alpha,\nu}$ of species α in the given frequency bin ν defined by (e.g., Osterbrock & Ferland 2006)

$$\Gamma_{\gamma\alpha,\nu} = \langle \sigma_{\alpha} \rangle_{\nu} \int_{\nu_1}^{\nu_h} d\nu \frac{4\pi J_{\nu}(\nu)}{h_{\text{P}}\nu}. \quad (9)$$

The photoionization rate implies a photoheating rate given by $\mathcal{E}_{\gamma\alpha,\nu} = \langle \varepsilon_{\alpha} \rangle_{\nu} \Gamma_{\gamma\alpha,\nu}$, where

$$\langle \varepsilon_{\alpha} \rangle_{\nu} = \left[\int_{\nu_1}^{\nu_h} d\nu \frac{4\pi J_{\nu}(\nu)}{h_{\text{P}}\nu} \sigma_{\alpha}(\nu) (h_{\text{P}}\nu - h_{\text{P}}\nu_{\alpha}) \right] \times \left[\int_{\nu_1}^{\nu_h} d\nu \frac{4\pi J_{\nu}(\nu)}{h_{\text{P}}\nu} \sigma_{\alpha}(\nu) \right]^{-1} \quad (10)$$

is the grey excess energy of frequency bin ν , and $h\nu_{\alpha}$ is the photoionization threshold energy of species α . For reference, $h\nu_{\text{HI}} = 13.6$ eV, $h\nu_{\text{HeI}} = 24.6$ eV, and $h\nu_{\text{HeII}} = 54.4$ eV.

¹ For brevity, we use the symbol ν both to number the frequency bin and to denote the frequency.

2.6.2 Secondary ionizations

The photoionization and photoheating rates are passed to the chemistry solver described above, which updates the abundances of hydrogen and helium that evolve according to the following set of equations (e.g., Kuhlen & Madau 2005),

$$\begin{aligned} \frac{d\eta_{\text{HI}}}{dt} &= \alpha_{\text{HII}} n_e \eta_{\text{HII}} - \eta_{\text{HI}} \Gamma_{\gamma\text{HI}} - \eta_{\text{HI}} \Gamma_{\text{eHI}} n_e \\ &- f_{\text{ion,HI}} \frac{(\eta_{\text{HI}} \mathcal{E}_{\text{HI}} + \eta_{\text{HeI}} \mathcal{E}_{\text{HeI}})}{13.6\text{eV}}, \end{aligned} \quad (11)$$

$$\begin{aligned} \frac{d\eta_{\text{HeI}}}{dt} &= \alpha_{\text{HeII}} n_e \eta_{\text{HeII}} - \eta_{\text{HeI}} \Gamma_{\gamma\text{HeI}} - \eta_{\text{HeI}} \Gamma_{\text{eHeI}} n_e \\ &- f_{\text{ion,HeI}} \frac{(\eta_{\text{HI}} \mathcal{E}_{\text{HI}} + \eta_{\text{HeI}} \mathcal{E}_{\text{HeI}})}{24.6\text{eV}}, \end{aligned} \quad (12)$$

$$\frac{d\eta_{\text{HeIII}}}{dt} = \eta_{\text{HeII}} \Gamma_{\gamma\text{HeII}} + \eta_{\text{HeII}} \Gamma_{\text{eHeII}} n_e - \alpha_{\text{HeIII}} n_e \eta_{\text{HeIII}}, \quad (13)$$

respecting the constraints

$$\eta_{\text{HI}} + \eta_{\text{HII}} = 1, \quad (14)$$

$$\eta_{\text{HeI}} + \eta_{\text{HeII}} + \eta_{\text{HeIII}} = \eta_{\text{He}}, \quad (15)$$

$$\eta_{\text{HII}} + \eta_{\text{HeII}} + 2\eta_{\text{HeIII}} = \eta_e, \quad (16)$$

where $\Gamma_{\text{e}\alpha}$ and α_{α} are the collisional ionization and recombination rate coefficients for species α . The helium abundance is defined as $\eta_{\text{He}} = n_{\text{He}}/n_{\text{H}} = X_{\text{He}}(m_{\text{H}}/m_{\text{He}})/(1 - X_{\text{He}})$ and m_{H} and $m_{\text{He}} = 4m_{\text{H}}$ are the masses of the hydrogen and helium atoms.

The factors $f_{\text{ion,HI}}$ and $f_{\text{ion,HeI}}$ describe the secondary ionizations of HI and HeI by energetic electrons. We use the ionization and energy dependent fits by Ricotti et al. (2002) to the results of Shull & van Steenberg (1985), i.e.,

$$\begin{aligned} f_{\text{ion,HI}} \approx &- 0.69 \left(\frac{28\text{eV}}{E} \right)^{0.4} \eta_e^{0.2} (1 - \eta_e^{0.38})^2 \\ &+ 0.39 (1 - \eta_e^{0.41})^{1.76}, \end{aligned} \quad (17)$$

$$f_{\text{ion,HeI}} \approx - 0.098 \left(\frac{28\text{eV}}{E} \right)^{0.4} \eta_e^{0.2} (1 - \eta_e^{0.38})^2 + 0.55(1 - \eta_e^{0.46})^{1.67}, \quad (18)$$

for $E > 28$ eV and $f_{\text{ion,HI}} = f_{\text{ion,HeI}} = 0$ for $E < 28$ eV, where $E = h_{\text{P}}(\nu - \nu_{\alpha})$ is the energy of the primary electron resulting from photoionizations of species α by photons with energy $h_{\text{P}}\nu$. We follow Ricotti et al. (2002) and neglect secondary ionization and excitation of HeII. Ricotti et al. (2002) also provided fits to the factors f_{heat} by which the rate at which the gas is photoheated must be reduced to account for the energy lost in secondary ionizations and excitations,

$$f_{\text{heat}} \approx 3.9811 \left(\frac{11\text{eV}}{E} \right)^{0.7} \eta_e^{0.4} (1 - \eta_e^{0.34})^2 + [1 - (1 - \eta_e^{0.27})^{1.32}], \quad (19)$$

for $E > 11$ eV and $f_{\text{heat}} = 1$ for $E < 11$ eV. Figure 1 compares the energy dependent fits by Ricotti et al. (2002) at a range of electron fractions with the Shull & van Steenberg (1985) high-energy limit that we employed in Jeon et al. (2012) independent of electron energy. The figure also shows the results of the more recent work by Furlanetto & Stoever (2010).

2.6.3 Numerical parameter choices

In the simulations presented in this work, we set $\tilde{N}_{\text{ngb}} = 32$, and choose an angular resolution of the transport of $N_{\text{TC}} = 128$ and of the merging of $N_{\text{RC}} = 8$. These choices have been made after carrying out a set of comparison runs and testing for convergence. Sources emit photons into $N_{\text{EC}} = 128$ directions using emission time steps $\Delta t_{\text{em}} = \min(10^{-3} \text{ Myr}, \Delta t_{\text{r}})$. Photons are transported at a speed $\tilde{c} = 0.1c$, where c is the speed of light, using time steps of size $\Delta t_{\text{r}} = \min(10^{-2} \text{ Myr}, \Delta t_{\text{hydro}})$, where Δt_{hydro} is the smallest GADGET particle time step. The reduction of the speed of light by a factor 10 does not noticeably affect the outcome of our simulations, but reduces the simulation cost. We use four unevenly spaced frequency bins with bounding energies located at [13.6, 24.6, 54.4, 400, 10^4] eV. Test runs using a larger number of frequency bins yielded nearly indistinguishable results, consistent with the discussion in Mirocha et al. (2012).

We use the fits to the frequency-dependent photoionization cross sections by Verner et al. (1996), and simplify the computation of the grey photoionization cross sections $\langle \sigma_{\alpha} \rangle_{\nu}$ and of the grey excess energies $\langle \varepsilon_{\alpha} \rangle_{\nu}$ by adopting a fixed spectrum independent of the source from which the photons in frequency bin ν originate. To improve on this approximation, we compute the grey averages using the spectrum of the source formed last, assuming accretion at the Eddington rate and a BH mass of $100 M_{\odot}$ in the case of X-ray sources. Tests in which we varied the adopted spectrum over the range of typical spectra of the sources suggested no significant impact of this approximation on our results. An accurate treatment in which individual grey cross-sections and excess energies are assigned to each photon packet will be pursued in future work. For simplicity, we do not compute grey averages of the energy dependent functions $f_{\text{ion,HI}}$, $f_{\text{ion,HeI}}$, and f_{heat} describing secondary ionization, but evaluate them at the

characteristic frequency determined by averaging the frequencies inside the bins weighted by the spectrum of the source.

To reduce the computational expense of the simulations we do not trace photons emitted by X-ray sources with accretion rates below $\dot{M}_{\text{BH}} < 10^{-10} M_{\odot} \text{ yr}^{-1}$. Tests showed that the radiative feedback from BHs with such low accretion rates is negligible, consistent with our discussion in Jeon et al. (2012). We also do not follow the propagation of photons outside the high-resolution region.

2.7 Photodissociation of H₂ and HD

The molecules H₂ and HD are photodissociated by LW photons with energies in the range 11.2 – 13.6 eV. We follow previous works (e.g., Wise & Abel 2008a; Wolcott-Green et al. 2011; Safranek-Shrader et al. 2012; Johnson et al. 2013; Agarwal et al. 2012) and compute the photodissociation rates in the optically thin limit and apply a shielding correction to approximate RT effects. The photodissociation rate of H₂ is thus (Abel et al. 1997)

$$k_{\text{H}_2} = 1.1 \times 10^8 \text{ s}^{-1} \frac{f_{\text{shield,H}_2} F_{\text{LW}}}{\text{erg Hz}^{-1} \text{ s}^{-1} \text{ cm}^{-2}} \quad (20)$$

and the photodissociation rate of HD is (Wolcott-Green & Haiman 2011)

$$k_{\text{HD}} = 1.1 \times 10^8 \text{ s}^{-1} \frac{f_{\text{shield,HD}} f_{\text{shield,H}_2,\text{HD}} F_{\text{LW}}}{\text{erg Hz}^{-1} \text{ s}^{-1} \text{ cm}^{-2}}, \quad (21)$$

where $F_{\text{LW}} = 4\pi J_{\text{LW}}$ is the flux in the LW bands computed in the optically thin limit, i.e., ignoring any absorption of the LW photons by the gas, and J_{LW} the corresponding intensity.

The dimensionless factors $f_{\text{shield,H}_2}$, $f_{\text{shield,HD}}$, and $f_{\text{shield,H}_2,\text{HD}}$ describe the local attenuation of the flux by self-shielding of H₂, self-shielding of HD, and shielding of HD by H₂. We compute the self-shielding factors $f_{\text{shield,H}_2}$ and $f_{\text{shield,HD}}$ using (Wolcott-Green et al. 2011)

$$f_{\text{shield}}(N, T) = \frac{0.965}{(1 + x/b_5)^{\alpha}} + \frac{0.035}{(1 + x)^{0.5}} \times \exp[-8.5 \times 10^{-4} (1 + x)^{0.5}], \quad (22)$$

where $x \equiv N_i/5 \times 10^{14} \text{ cm}^{-2}$, N_i is the column density of the molecule species, $b_5 \equiv b/10^5 \text{ cm s}^{-1}$, $b \equiv \sqrt{2k_{\text{B}}T/m_{\text{p}}}$ the Doppler broadening parameter, $m_{\text{p}} = 2m_{\text{H}}$ the mass of the molecule species, and $\alpha = 1.1$. We compute the factor $f_{\text{shield,H}_2,\text{HD}}$ that describes shielding of HD by H₂ using (Wolcott-Green et al. 2011)

$$f_{\text{shield,H}_2,\text{HD}} = \frac{1}{(1 + x)^{0.238}} \exp(-5.2 \times 10^{-3} x), \quad (23)$$

where $x \equiv N_{\text{H}_2}/2.34 \times 10^{19} \text{ cm}^{-2}$. The column density N is estimated using $N = nL_{\text{char}}$, where n is the number density of the molecule species and L_{char} the characteristic length scale. We set the latter equal to the local Jeans length, an approximation that is appropriate for self-gravitating systems (Schaye 2001a; Schaye 2001b) and that performs well in comparison with more sophisticated approaches (e.g., Wolcott-Green et al. 2011).

For reference, the LW intensity of a single Pop III star at distance r , computed in the optically thin limit, is $J_{\text{LW},21} \approx 0.1(r/1.6 \text{ kpc})^{-2}$, where $J_{\text{LW},21} \equiv$

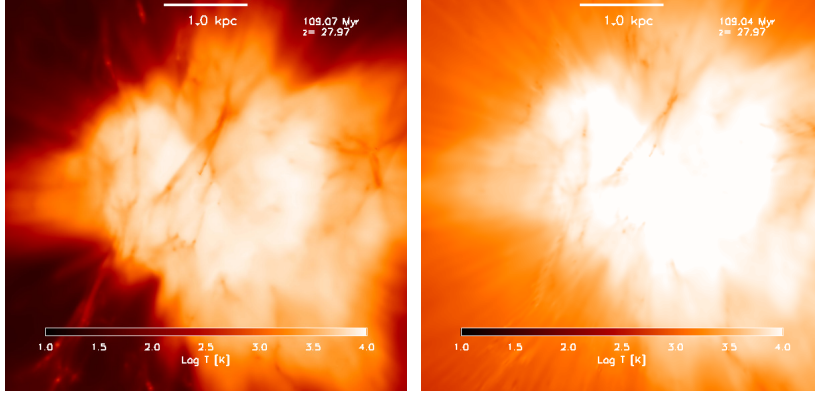


Figure 2. Temperatures, averaged along the line of sight, in a cubical cutout of linear extent 150 comoving kpc centred on the first sink particle 2 Myr after the formation of the first BH, in the simulation in which the BH grew by accreting diffuse halo gas (*left*), and in the simulation in which the BH grew by accretion from the stellar companion in a HMXB (*right*). In the former case, because of the low Bondi-Hoyle accretion rates, the ionizing luminosities are negligible, and the butterfly-shaped photoheated relic HII region created by the Pop III progenitor star dominates the image. In the latter case, on the other hand, the large X-ray luminosity of the HMXB implies a strong preheating of the IGM outside of the stellar relic HII region.

$J_{\text{LW}}/(10^{-21} \text{ erg s}^{-1} \text{ cm}^{-2} \text{ Hz}^{-1} \text{ sr}^{-1})$. The LW flux from an accreting BH depends on the accretion rate and the BH mass. For a $100 M_{\odot}$ BH with typical Bondi-Hoyle accretion rates of $10^{-8} M_{\odot} \text{ yr}^{-1}$ we have $J_{\text{LW},21} \approx 5.3 \times 10^{-5} (r/1.6 \text{ kpc})^{-2}$. The flux of LW radiation implied by a single HMXB with a BH mass of $100 M_{\odot}$ and accreting at the Eddington rate is $J_{\text{LW},21} \approx 4 \times 10^{-3} (r/1.6 \text{ kpc})^{-2}$.

3 RESULTS

In the following, we investigate how the impact of radiative feedback on Pop III star formation and the early IGM varies between the simulations with and without HMXBs. First, in Section 3.1, we discuss the feedback of the first HMXB on the gas in and around its minihalo host. Then, in Section 3.2, we investigate how the presence of HMXBs affects the cosmic star formation history. In Section 3.3, we study the effects on the IGM, and in Section 3.4, we study the effects on the gas in haloes in the two simulations with and without HMXBs. In Sections 3.5 and 3.6 we discuss the implications of feedback from HMXBs for reionization and BH growth.

We emphasize that both simulations account for the radiative feedback from Pop III stars and from BHs accreting diffuse halo gas. The comparison presented here thus elucidates the impact of radiative feedback by HMXBs complementing the radiative feedback from Pop III stars and miniquasars in a simulation of the formation of the first stars and galaxies.

3.1 Gas properties in the first minihalo

In both runs, the first stellar binary forms at $z = 28$; the runs are identical up to this redshift. The formation time and the size of the HII region with radius $\sim 2 - 3$ kpc are consistent with previous works (e.g. Kitayama et al. 2004; Yoshida et al. 2007; Abel et al. 2007; Greif et al. 2009). The density profile of the surrounding gas and specifically the location of the shock driven by the photoevaporating

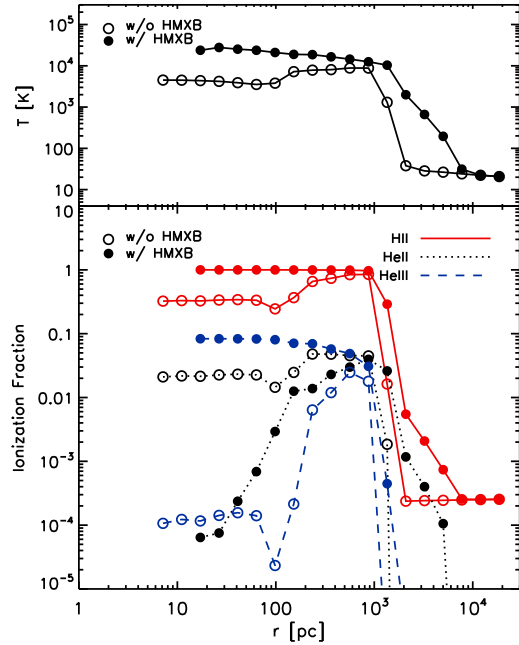


Figure 3. Spherically averaged profiles of the temperature and ionization fractions in the simulations with (open circles) and without (filled circles) HMXBs at 2 Myr after the formation of the BH, the same time as in Figure 2. In the simulation without HMXBs, the relic HII region left behind the first Pop III star has started to recombine and cool. Recombination is enhanced in the dense photo-evaporation shock located at $r = 100$ pc. The HMXB keeps the gas inside the relic stellar HII region ionized and hot, and preionizes and preheats the IGM ahead of the stellar ionization front. Ionization by the hard HMXB spectrum implies a strong increase in the fraction of doubly ionized helium.

gas from the minihalo host are in good agreement with the results of our earlier simulations in Jeon et al. (2012) which started from identical initial conditions.

In Figure 2, we compare images of the gas temperature

2 Myr after the collapse of the primary into a BH of mass $100 M_{\odot}$ in the two simulations. In both simulations, the gas in the relic stellar HII region has been heated to $\sim 10^4$ K by the Pop III progenitor. In the simulation without HMXBs, accretion of gas on the BH occurs at a rate too low to sustain the high ionization of the gas (see Figure 9 discussed in Section 3.6), and the relic HII region recombines and cools. In the simulation with HMXBs, on the other hand, thanks to the large X-ray luminosity of the first HMXB, the gas in the relic HII region is kept highly ionized and at $\sim 10^4$ K, and in addition, there is a significant heating of the gas ahead of the stellar ionization front.

In Figure 3 we quantify the impact of the first HMXB on the spherically averaged properties of the halo gas at 2 Myr after the collapse of the primary into a BH, the same time as in Figure 2. Owing to the slight overdensity at the position of the photoevaporation shock, gas recombination occurs at an increased rate around ~ 100 pc from the source, which explains the dip in the ionized fractions. The enhanced ionization beyond the I-front in the presence of the HMXB is mostly due to secondary ionization of HI by electrons generated in absorptions of X-rays by HeI (Figure 1; Machacek et al. 2003; Madau et al. 2004). The efficient ionization by X-rays emitted by the HMXB implies a strong increase in the abundances of HeIII with respect to that in the simulation without HMXBs. The radii of the HeII and HeIII regions are only slightly smaller than that of the HII region, consistent with the results in Venkatesan & Benson (2011).

3.2 Star formation history

It has been suggested that preionization of gas by the absorption of X-rays may promote the formation of molecular hydrogen and increase the ability of the gas to cool and form stars (Haiman et al. 2000; see also, e.g., Ricotti et al. 2001). Several studies have now confirmed this possibility (e.g., Machacek et al. 2003; Glover & Brand 2003; Kuhlen & Madau 2005). However, the positive feedback from X-ray ionization on the formation of molecular hydrogen needs to compete with the negative radiative feedback caused by pressure-smoothing in the photoheated gas (e.g., Shapiro et al. 1994; Thoul & Weinberg 1996; Gnedin 2000; Dijkstra et al. 2004; Mesinger & Dijkstra 2008; Okamoto et al. 2008; Wise & Abel 2008b; Pawlik & Schaye 2009; Petkova & Springel 2011; Sobacchi & Mesinger 2013), and also with the negative feedback from LW photons dissociating molecular hydrogen (e.g., Haiman et al. 1997; Machacek et al. 2001; Ahn & Shapiro 2007; O’Shea & Norman 2008). Accordingly, most investigations found at most a modest net positive impact of X-ray ionization on gas collapse, even in the absence of a strong LW background (e.g., Glover & Brand 2003; Kuhlen & Madau 2005). Consistent with these earlier works, in Jeon et al. (2012), we found that X-ray ionization by the first BHs generates at most a modest increase in the star formation rate in simulations of high-redshift minihaloes. The exception was an initial brief phase of significantly increased star formation in an idealized simulation of ionization by a HMXB.

Figure 4 compares the formation histories of Pop III stars and the associated comoving star formation rate densities in our current simulations with and without HMXBs. There is little difference between the two simulations, and

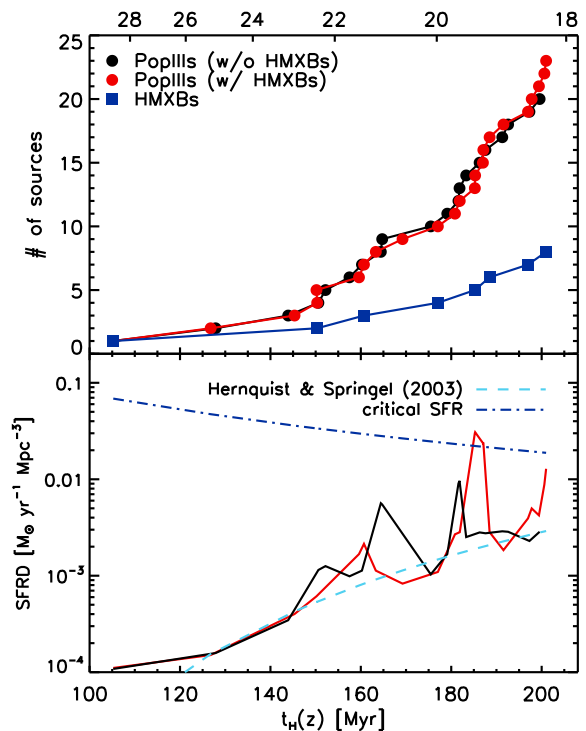


Figure 4. *Top:* cumulative number of Pop III binaries in the runs with (red) and without (black) HMXBs, and cumulative number of HMXBs (blue squares). The number of stars formed is similar in the two simulations, and hence there is no strong net feedback by HMXBs. *Bottom:* comoving star formation rate densities in the two simulations. For comparison, we also show the fit to the star formation rate density by Hernquist & Springel (2003, light blue dashed). The blue dash-dotted curve shows a lower limit to the critical star formation rate density needed to sustain ionization of the IGM, computed using Equation 24 and assuming $C/f_{\text{esc}} = 1$.

hence we find no significant net radiative feedback from HMXBs on the star formation rate. This is consistent with the lack of a strong net radiative feedback on the star formation history from either accreting BHs or HMXBs at $z \lesssim 20$ in Jeon et al. (2012). However, our current simulations do not reproduce the strong early enhancement in the star formation rate at $z \gtrsim 20$ in the presence of HMXBs seen in the simulation BHB of Jeon et al. (2012), despite their identical initial conditions. The lack of an early phase of a net positive feedback by HMXBs on star formation likely owes to our adoption of a physically more realistic model of the formation of HMXBs in the current simulations, as we now explain.

In Jeon et al. (2012), we followed the radiative feedback from a single HMXB continuously emitting X-ray photons throughout the simulation. In the current work, on the other hand, there are 4 HMXBs forming at $z > 20$ (see Figure 4). However, each of them emits radiation for only a brief interval of 2 Myr, which in total corresponds to just about a tenth of the time during which the HMXB was active in our previous simulation at $z > 20$. The lack of a net positive feedback on early star formation in the current simulation is consistent with this reduced duty cycle for emission of X-rays by HMXBs. Indeed, Figure 4 shows that near the

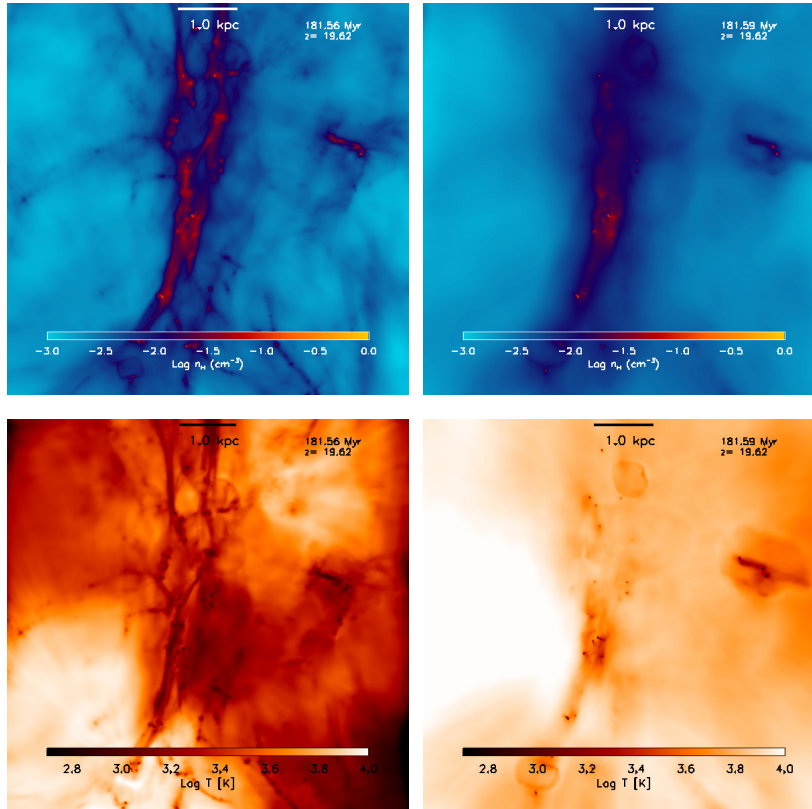


Figure 5. Hydrogen number densities (*top*) and temperatures (*bottom*) at $z = 19.6$, averaged along the line of sight, in a cubical cutout of linear extent 300 comoving kpc centred on the first sink particle, in the simulations without (*left*) and with (*right*) HMXBs. The stronger photo-ionization heating in the presence of HMXBs and the associated increase in the thermal gas pressure imply a stronger smoothing of the gas density field.

end of the simulation, at $z \lesssim 20$, when HMXB formation occurs more frequently at an average rate of about once in 5 Myr, the star formation rates in the current simulation with HMXBs are slightly higher than those in the simulation without HMXBs.

In the current work we find 19 sink particles at the end of the simulation without HMXBs at $z \approx 18$. This is a larger number than the 11 sink particles found at the same redshift in our previous simulation BHS in Jeon et al. (2012) that included persistent X-ray radiation from an isolated BH miniquasar accreting diffuse halo gas and that started from identical initial conditions. We identify two key differences in the simulation methodology to explain this difference in star formation rates. First, in the current work, we account for shielding of the primordial molecular gas from LW photons that was ignored in the previous simulations. LW feedback is therefore less effective in the present work than in the previous simulations and this promotes gas cooling and condensation. Second, in Jeon et al. (2012), we overestimated the radii of HII regions around Pop III stars by a factor of ~ 2 as a result of a numerical error discussed in Jeon et al. (2012). Thus, in the current work, the suppression of star formation by stellar ionizing radiative feedback is expected to be weaker than in the preceding paper.

It is interesting to compare the simulated star formation rate densities with the comoving critical star formation rate

density to sustain ionization against recombinations (Madau et al. 1999),

$$\rho_{\text{SFR,crit}} = 0.02 \text{ M}_{\odot} \text{ yr}^{-1} \text{ Mpc}^{-3} \left(\frac{C}{f_{\text{esc}}} \right) \left(\frac{1+z}{20} \right)^3, \quad (24)$$

where $C \equiv \langle n_{\text{H}}^2 \rangle / \bar{n}_{\text{H}}^2$ is the clumping factor that parametrizes the recombination rate in the IGM (e.g., Madau et al. 1999; Miralda-Escudé et al. 2000; Wise & Abel 2005; Pawlik et al. 2009; Finlator et al. 2012; Shull et al. 2012), the brackets indicate the volume-weighted average, \bar{n}_{H} is the cosmological mean gas density, and f_{esc} is the fraction of ionizing photons that escape haloes to ionize the IGM (e.g., Razoumov & Sommer-Larsen 2006; Gnedin et al. 2008; Wise & Cen 2009; Paardekooper et al. 2011; Yajima et al. 2011). Figure 4 shows that the simulated star formation rate densities are generally below the critical star formation rate density, indicating that the reionization of the simulated high-resolution region remains incomplete. Because, typically, $C > 1$ (see Section 3.3) and, by definition, $f_{\text{esc}} \leq 1$, we have conservatively underestimated the ratios of critical and simulated star formation rate densities.

3.3 Effects of HMXBs on IGM properties

Figure 5 shows images of the gas density and temperature in the high-resolution region centred on the site of formation of the first stellar binary near the end of the simulation

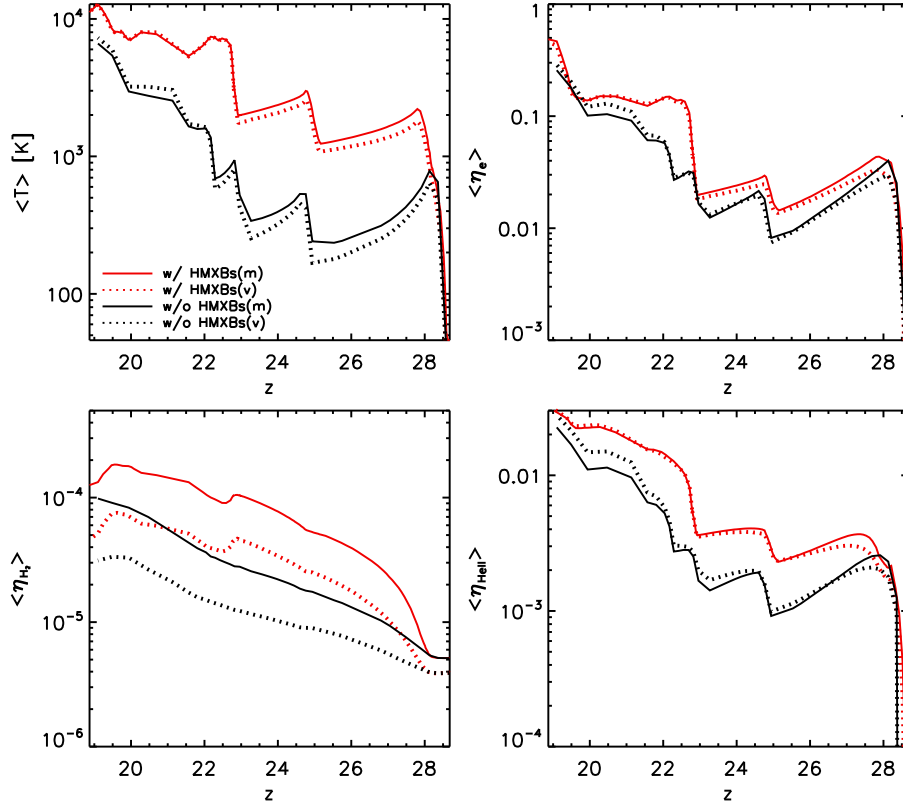


Figure 6. The properties of the gas in the high-resolution region of the simulations with (red) and without (black) HMXBs. The individual panels show, from left to right and top to bottom, temperature, electron fraction, molecular hydrogen fraction, and HeII fraction. Solid (dotted) curves show mass-weighted (volume-weighted) averages. HMXBs preionize and preheat the gas. The increased electron fraction promotes the formation of molecular hydrogen. Ionization by the hard HMXB spectrum generates an increased abundance of HeII.

at $z = 19.6$. In the simulation that included ionization by HMXBs, the gas is photoheated to temperatures in excess of a few times $\sim 10^3$ K throughout the simulation volume. In the simulation without HMXBs, which misses the bright HMXB phases of the accreting BHs, on the other hand, the average temperature is significantly lower, and heating to comparably high temperatures is limited to volumes inside stellar HII regions. The higher temperatures in the simulation with HMXBs imply a cosmological Jeans mass (e.g., Shapiro et al. 1994; Gnedin 2000; Wise & Abel 2008a) and hence a smoothing of the gas density field by thermal pressure that is visibly larger than in the simulation without HMXBs (see Section 3.5 for a quantitative discussion).

Figure 6 quantifies the evolution of the properties of the gas averaged within the high-resolution region in the two simulations. The additional ionization by the hard radiation emitted by HMXBs increases the fraction of HeII with respect to the fractions found in the absence of HMXBs. The electron fraction is increased in the simulation with HMXBs over that in the simulation without HMXBs, largely owing to secondary ionization of hydrogen (see Section 3.1). The fraction of the primary electron energy that is used in secondary ionizations decreases with increasing electron fraction and instead heats the gas (Figure 1; e.g., Shull & van Steenberg

1985; Furlanetto & Stoever 2010). Thus, once the local electron fraction becomes $\gtrsim 0.1$, further ionization is dominated by stellar radiation (e.g. Mesinger et al. 2013). The increased electron fraction in the simulation with HMXBs promotes the formation of H_2 , in agreement with earlier work (Kuhlen & Madau 2005; see also, e.g., Haiman et al. 2000; Machacek et al. 2003; Ricotti & Ostriker 2004). Near the end of the simulations, when stellar radiation contributes significantly to photoionization and dissociation of H_2 , the temperatures and species fractions become similar in both simulations.

3.4 Effect of HMXBs on gas properties in haloes

In Figure 7 we compare the properties of the gas inside haloes in the simulations with and without HMXBs. Haloes were extracted from the high-resolution region displayed in Figure 5 at $z = 19.6$ using the halo finder SUBFIND (Springel et al. 2001) and adopting a linking length equal to a fifth of the mean inter-particle distance in the high-resolution region to generate friends-of-friends (FOF) particle group catalogues. Each circle in Figure 7 shows the mass-weighted average of the corresponding gas particle property inside the virial sphere with radius r_{200} centred on the most-

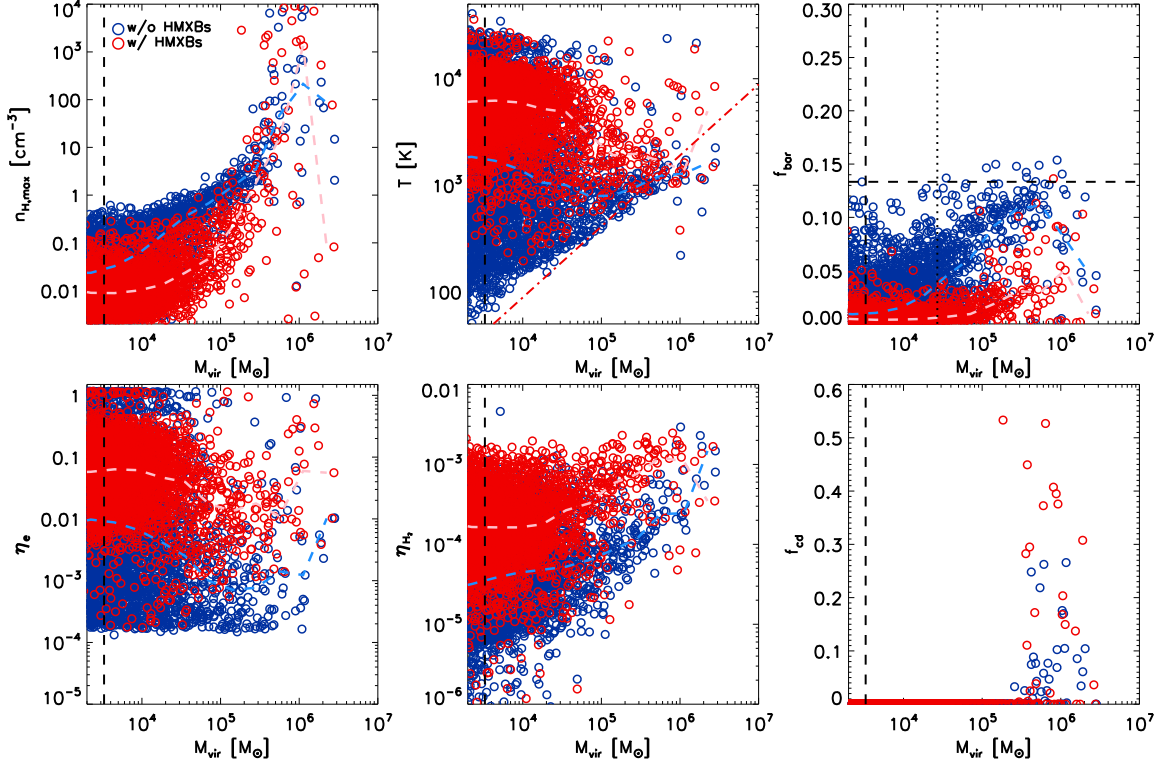


Figure 7. Properties of the gas inside haloes at $z = 19.6$ for the simulations without (blue circles) and with (red circles) HMXBs. The dashed curves of matching color show the median relations to guide the eye. The individual panels show, from left to right and top to bottom, the maximum hydrogen number density, the mass-weighted average molecular hydrogen fraction, and the fraction of cold dense gas ($T \leq 0.5T_{\text{vir}}$ and $n_{\text{H}} \geq 10^4 \bar{n}_{\text{H}} \approx 20 \text{ cm}^{-3}$). The vertical dashed lines mark the mass of 100 DM particles. The red dashed-dotted line in the top middle panel indicates the virial temperature T_{vir} assuming a mean particle weight $\mu = 1.2$, appropriate for mostly neutral gas. The vertical dotted line in the top right panel marks the cosmological Jeans mass above which gravitational attraction dominates pressure repulsion and haloes can accrete gas. In the presence of HMXBs, the temperatures, electron fractions, and molecular hydrogen fractions are strongly increased. The HMXBs exert a strong feedback on the baryon fractions, which are strongly suppressed below the cosmic mean (horizontal dashed line) across the range of halo masses. However, the feedback from HMXBs on the fraction of cold dense gas is only mild, and the number of haloes above the critical mass for the onset of cooling and star formation is similar with and without HMXBs, consistent with the lack of a strong net feedback from HMXBs on the star formation history (Figure 4).

bound particle of the main subhalo inside a given FOF particle group.

Several halo properties are similar in both simulations. For instance, the maximum hydrogen number density $n_{\text{H,max}}$ shows an abrupt increase with increasing halo mass above $M_{\text{vir}} \gtrsim 3 \times 10^5 M_{\odot}$. This is caused by the increased ability of haloes above this mass to form H_2 and to cool and condense the gas (e.g., Tegmark et al. 1997; Machacek et al. 2001; Yoshida et al. 2003; O’Shea & Norman 2008). Indeed, the characteristic fraction of molecular hydrogen features an increase with halo mass near this mass scale. The lowest mass haloes have characteristic temperatures in excess of the virial temperature expected for their mass as their gas is photoionized by stellar radiation from nearby stars. Halos with mass below the cosmological Jeans mass, evaluated at the cosmic mean density and the cosmic mean temperature expected in the absence of star formation (e.g., Gnedin 2000), have baryon fractions substantially below the cosmic mean. The most massive minihaloes achieve baryon fractions

closer to the cosmic mean, but also at these masses the scatter is large, owing to stellar radiative feedback and gravitational and gas-dynamical interactions between haloes (e.g., Wise & Abel 2008b; Wise et al. 2012; Pawlik et al. 2013).

The presence of HMXBs leaves clear signatures in the halo gas properties. The characteristic temperatures and electron fractions are significantly increased at all mass scales. The increased electron fraction results in an enhancement of the molecular hydrogen fraction by an order of magnitude compared to that in the simulation without HMXBs in all but the most massive haloes. Furthermore, the baryon fractions are significantly lower in the simulation with HMXBs than without, even at the largest halo masses. The reason for this is that X-ray preheating helps stellar radiative feedback by evaporating halo gas and suppressing baryonic infall onto haloes (e.g., Machacek et al. 2003; Kuhlen & Madau 2005; Jeon et al. 2012). However, the presence of HMXBs does not hinder the build-up of cold dense gas cores in the centres of haloes that fuel the formation of

stars. Here, the cold and dense gas is defined as the gas with $T \lesssim 0.5T_{\text{vir}}$ and $n_{\text{H}} \gtrsim 10^4 \bar{n}_{\text{H}}$ where $\bar{n}_{\text{H}} \approx 1.7 \times 10^{-3} \text{ cm}^{-3}$ is the cosmic mean gas density at $z = 19.6$ (cf. Machacek et al. 2003).

The mild impact on the cold dense gas suggests that the reduction in the baryon fraction originates mostly in the outer lower density regions of the haloes and is consistent with the lack of a strong net effect of HMXBs on the star formation history. In principle, the increase in H_2 can help the collapse of the gas in haloes by increasing the ability of the primordial gas to cool. Indeed, the simulation including HMXBs shows an increased amount of cold dense gas for haloes above the critical mass for the onset of efficient cooling. However, the number of haloes with cold gas fraction $\gtrsim 0.1$ is similar in both our simulations. Moreover, the critical mass for the onset of cooling is insensitive to the presence of HMXBs, and above this mass molecular hydrogen formation is already very efficient in the absence of additional positive feedback.

Our results are consistent with the results of Machacek et al. (2003) and Kuhlen & Madau (2005), both of which investigated the feedback from X-ray ionization on structure formation and halo gas properties in cosmological simulations of high-redshift minihaloes. Varying the strength of the X-ray flux by two orders of magnitude with respect to the intensity of the imposed LW background, Machacek et al. (2003) found only a mild effect on the ability of gas to cool and collapse to high densities. Even a high X-ray flux was found to be insufficient to substantially increase the fraction of cold dense gas or to significantly lower the critical halo mass for the onset of efficient gas cooling. A similar insensitivity of the cold dense gas fractions to X-ray ionization was found in Kuhlen & Madau (2005) and attributed to the competition with the negative feedback from photoheating.

3.5 Reionization

It is generally accepted that the stellar radiation from galaxies is mainly responsible for the reionization of the Universe (for reviews see, e.g., Barkana & Loeb 2001; Barkana 2009; Robertson et al. 2010). However, X-ray sources, such as BHs, HMXBs, and structure formation and supernova remnant shocks (e.g. Oh 2001; Madau et al. 2004; Ricotti & Ostriker 2004; Ripamonti et al. 2008; Power et al. 2009; Johnson & Khochfar 2011; McQuinn 2012; Mirabel et al. 2011; Haiman 2011; McQuinn 2012; Mesinger et al. 2013; Fialkov et al. 2014), could have established a floor of ionized fractions of ~ 10 per cent nearly uniformly throughout the Universe and preheated the IGM to a few times $\sim 10^3$ K (e.g. Oh 2001; Volonteri & Gnedin 2009; Johnson & Khochfar 2011; McQuinn 2012; Mesinger et al. 2013). The associated X-ray feedback may delay reionization by impeding galaxy formation due to photoionization heating (e.g., Efstathiou 1992; Shapiro et al. 1994; Gnedin 2000; Finlator et al. 2011). Or it may accelerate it, by reducing the clumping factor of the IGM, and hence the number of ionizing photons required to keep the Universe ionized (e.g., Wise & Abel 2005; Pawlik et al. 2009), or by promoting the formation of molecular hydrogen (Haiman et al. 2000; see also, e.g., Ricotti et al. 2001; Oh & Haiman 2002)

In Jeon et al. (2012) we showed that radiative feedback from the Pop III progenitor stars strongly reduces the Bondi-

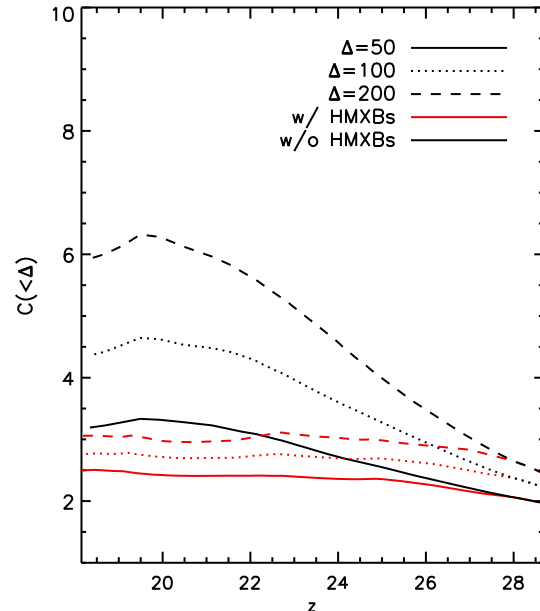


Figure 8. The volume-weighted clumping factor of gas with overdensities $\leq \Delta$. HMXBs preionize and preheat the gas, implying a strong smoothing of the diffuse IGM, reducing its clumpiness. This makes it easier to keep the gas ionized, and hence provides a positive feedback on reionization.

Hoyle rates at which BHs accrete diffuse gas in the first minihaloes (see also, e.g., Alvarez et al. 2009). Accordingly, the initial radiative impact of these BHs on the gas was found to be small. This is consistent with the results from our current simulation without HMXBs, in which many properties of the gas in the IGM and in the haloes are similar to those found in simulations of the first stars and galaxies that do not include the emission of X-rays by accreting BHs. The X-ray luminosities of HMXBs, on the other hand, are insensitive to the radiative feedback from the Pop III progenitor stars, as mass accretion occurs at high, near-Eddington rates directly from the stellar companion. As a result, we find that HMXBs substantially preionize and preheat the gas ahead of the ionization fronts driven by the first stars already at early times at which the radiative impact from BHs accreting diffuse gas is still negligible.

A key quantity for discussing reionization is the clumping factor C , which parametrizes the recombination rate in the IGM (see Section 3.2). Figure 8 shows the clumping factor computed by considering only gas with overdensities $\Delta \equiv n_{\text{H}}/\bar{n}_{\text{H}} \leq \Delta_{\text{IGM}}$ characteristic of the IGM, where \bar{n}_{H} is the cosmic mean density. We adopt $\Delta_{\text{IGM}} = 100$ as reference, and show the sensitivity of the clumping factor to changes in Δ_{IGM} by a factor of 2 above and below the reference value. The clumping factor is substantially smaller in the run with HMXBs than without, confirming the visual impression of pressure smoothing in Figure 5. The evolution of the clumping factor in the absence of HMXBs, when gas temperatures are determined mostly by stellar radiative feedback, is consistent with that in Wise & Abel (2008a). In their simulations, radiative feedback from the first stars decreased the gas clumpiness by ~ 25 per cent compared

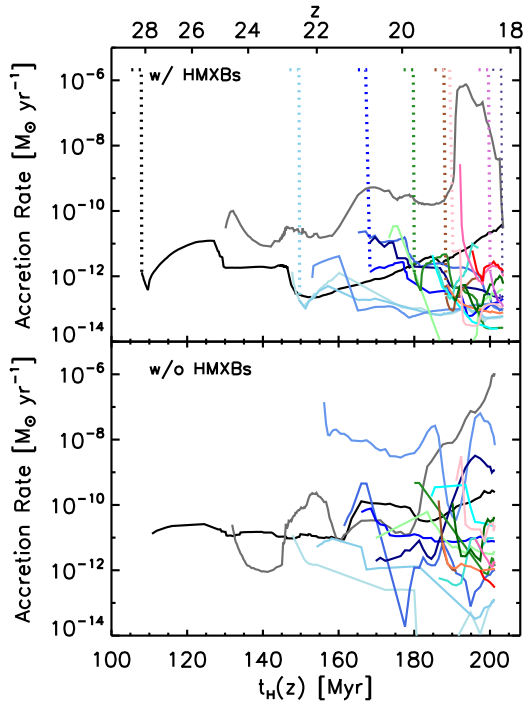


Figure 9. BH accretion rates in the simulations with (*top*) and without (*bottom*) HMXBs. The solid curves show the Bondi-Hoyle rates at which isolated BHs accrete diffuse halo gas. The dotted curves show the Eddington rates, $2.2 \times 10^{-6} M_{\odot} \text{ yr}^{-1} (M_{\text{BH}}/100 M_{\odot})$, of BHs accreting gas from the stellar companion in an HMXB. Stellar radiative feedback from the Pop III progenitor stars strongly reduces the rate of accretion of diffuse gas several orders of magnitude below the Eddington rate. HMXB feedback typically leads to an additional suppression of the Bondi-Hoyle accretion rates by a factor of a few.

to that in a comparison run without star formation. Our work demonstrates that in the presence of X-ray heating by HMXBs, the gas clumpiness can be reduced by an additional significant factor of ~ 2 .

In our current simulations, the rate at which stars form is insensitive to the presence of HMXBs (Figure 4). As discussed earlier, this is likely because the positive feedback by X-ray ionization on the formation of molecular hydrogen and the cooling of the primordial gas is partially offset by the negative feedback from photoheating and Jeans smoothing (Figure 7; e.g., Machacek et al. 2003; Kuhlen & Madau 2005). On the other hand, the presence of HMXBs leads to a significant reduction in the clumping factor of the IGM (Figure 8), and hence in the number of ionizing photons required to sustain ionization in the HII regions blown by the first stars. Our simulations therefore demonstrate that ionization by HMXBs can provide a significant net positive feedback on reionization. Such a net positive feedback has sometimes been assumed to operate in semi-analytic models (e.g., Madau et al. 2004; Mirabel et al. 2011).

3.6 Black hole growth

Observations of supermassive BHs (SMBHs) at $z \gtrsim 6$ (for reviews see, e.g., Fan et al. 2006; Willott et al. 2010; Mortlock

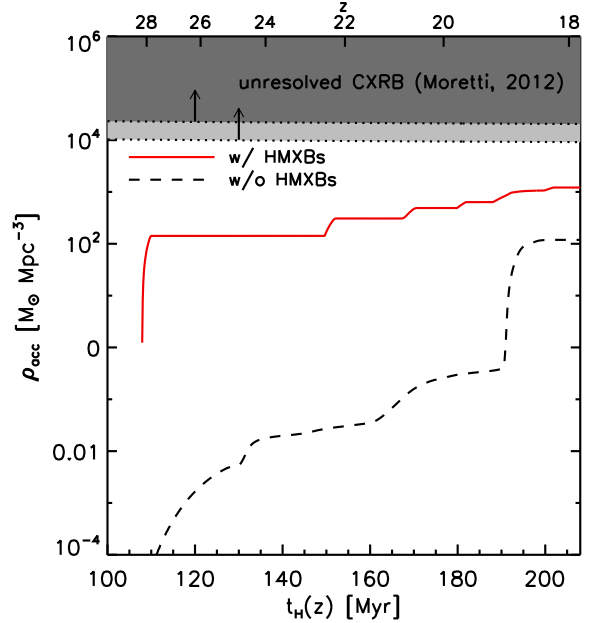


Figure 10. Comoving mass density accreted onto BHs in the simulations with (red solid) and without (black dashed) HMXBs. The shaded area marks the upper limit on the mass accretion density above $z > 5$ allowed by the unresolved CXRB (Moretti et al. 2012), as computed in Salvaterra et al. (2012), without (dark shaded) and with (light shaded) the contribution from faint sources at $z < 5$. The simulated comoving mass accretion densities are consistent with the observational constraints. However, they may violate these constraints if extrapolated to $z = 5$, implying a tension between CXRB limits and models of BH growth highlighted in Salvaterra et al. (2012).

et al. 2011) have triggered the question of their assembly. Various scenarios for SMBH formation have been suggested (for a recent review see Volonteri & Bellovary 2012), including the growth from a Pop III stellar-mass seed BH by gas accretion and mergers with other stellar mass BHs. A strong obstacle to this formation path is provided by the feedback from the first stars in the galaxies hosting the BHs, impeding gas accretion and delaying BH growth for ~ 100 Myr (e.g., Johnson & Bromm 2007; Pelupessy et al. 2007; Alvarez et al. 2009; Jeon et al. 2012; Johnson et al. 2013), and by the feedback from the BHs themselves (e.g., Milosavljević et al. 2009; Alvarez et al. 2009; Park & Ricotti 2011; Jeon et al. 2012). However, only a small fraction of all haloes needs to experience runaway BH growth to reach the observed space density of SMBHs at $z \gtrsim 6$ (e.g., Dijkstra et al. 2008; Tanaka et al. 2012; Johnson et al. 2013).

Figure 9 shows the gas accretion rates onto BHs in our two simulations with and without HMXBs. The Bondi-Hoyle accretion rates are up to ~ 8 orders of magnitude below the Eddington limit of $2.2 \times 10^{-6} M_{\odot} \text{ yr}^{-1} (M_{\text{BH}}/100 M_{\odot})$. This owes primarily to the feedback from the Pop III stars, but in the simulation with HMXBs, the Bondi-Hoyle accretion rates are suppressed, on average, to still lower values by feedback from X-ray heating. Interestingly, in both simulations, near the final simulation redshift, one of the BHs reaches diffuse accretion rates close to the Eddington rate, triggered by the passage through dense clouds of gas. Such

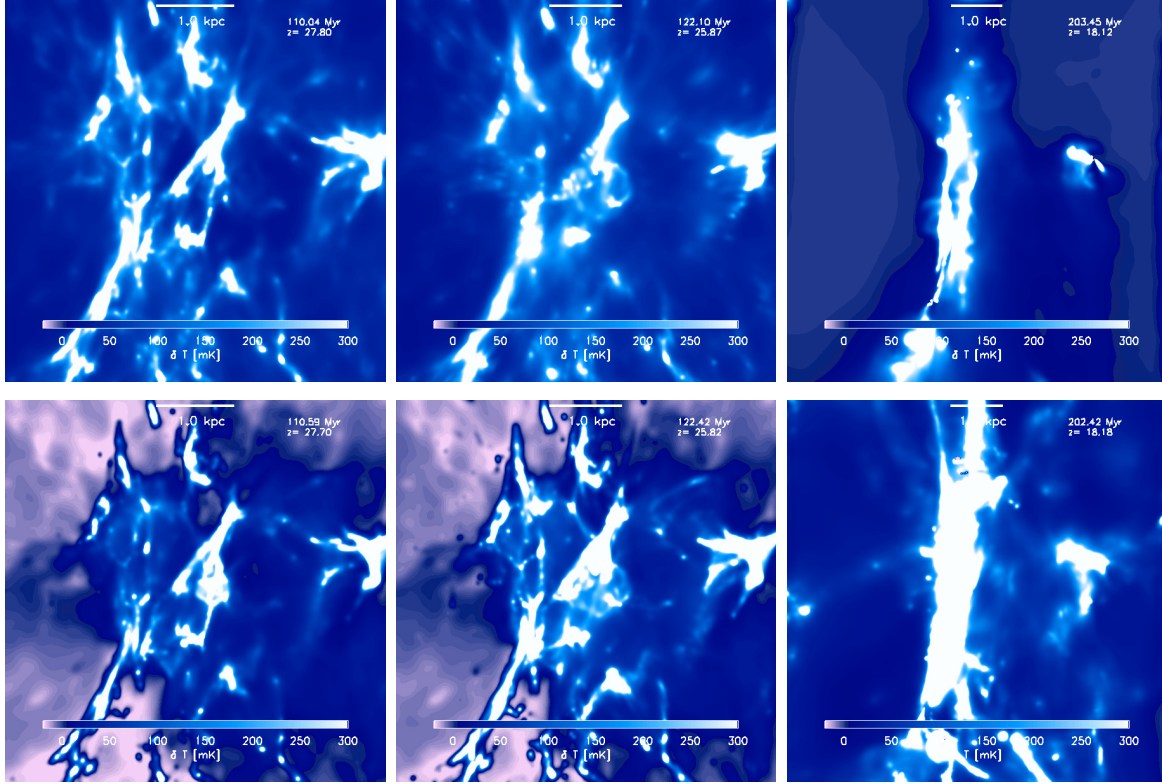


Figure 11. 21 cm differential brightness temperatures δT_b at $z = 27.8, 25.9$, and 18.1 (from left to right), averaged along the line of sight, in cubical cutouts of linear extent 300 comoving kpc centred on the first sink particle, in the simulations with (*top*) and without (*bottom*) HMXBs. The computation assumed that the spin temperature is equal to the gas temperature, $T_s = T_{\text{gas}}$, as may be expected after the establishment of a Ly- α background by the first stars. At early times (left and middle panels), in the absence of HMXBs, there is no significant preheating of the IGM outside the stellar HII regions, and the neutral IGM is seen in 21 cm absorption ($\delta T_b < 0$). In contrast, in the presence of HMXBs, X-ray preheating quickly establishes a nearly uniform temperature floor, and the neutral gas outside stellar HII regions is seen in 21 cm emission ($\delta T_b > 0$). At late times (right panels), the gas in the simulation with HMXBs is highly ionized and the 21 cm signal of the IGM nearly vanishes. In contrast, in the absence of HMXBs, the IGM outside stellar HII regions remains significantly neutral and is visible in 21 cm emission. The systematic differences in the differential brightness temperature of the IGM may potentially be used to constrain the nature of the first sources in upcoming 21 cm observations.

near-Eddington accretion could be characteristic of BHs residing in rare, high-density peaks in which self-gravity overcomes the feedback effects (e.g., Li 2011).

Measurements of the cosmic X-ray background (CXRB) have been used to constrain the population of high-redshift X-ray sources (e.g., Dijkstra et al. 2004; Ricotti & Ostriker 2004; Salvaterra et al. 2007; Treister et al. 2011; McQuinn 2012; Salvaterra et al. 2012; Dijkstra et al. 2012). Salvaterra et al. (2012) used the *Swift* X-ray telescope data in the hard X-ray band (Moretti et al. 2012) to obtain a limit of $\rho_{\text{acc}} \lesssim 1.4 \times 10^4 M_{\odot} \text{Mpc}^{-3}$ on the mass density accreted by BHs above $z \geq 5$, adopting the AGN spectra proposed by Sazonov et al. (2004) and a radiative efficiency $\epsilon = 0.1$. The dark shaded area in Figure 10 shows this upper limit extrapolated to high redshifts using their equation 7. The light-shaded area shows the corresponding reduced upper limit, discussed in Salvaterra et al. (2012), of $\rho_{\text{acc}} \lesssim 6.6 \times 10^3 M_{\odot} \text{Mpc}^{-3}$ at $z = 5$, now accounting for the contribution from faint sources at $z \lesssim 5$, as modeled in Gilli et al. (2007).

The simulated comoving accretion mass densities onto BHs and HMXBs shown in Figure 10 are computed using

$$\rho_{\text{acc}} = \int_{z=30}^{z=18} dt \sum_{\text{all}} (\dot{\rho}_{\text{acc,BH}} + \dot{\rho}_{\text{acc,HMXB}}), \quad (25)$$

where $\dot{\rho}_{\text{acc,BH}}$ is the time-dependent accretion mass density onto BHs accreting diffuse halo gas, and $\dot{\rho}_{\text{acc,HMXB}}$ is the time-independent accretion rate density onto BHs of mass $100 M_{\odot}$ inside HMXBs accreting gas from the stellar companion at the Eddington rate, $2.2 \times 10^{-6} M_{\odot} \text{yr}^{-1} (M_{\text{BH}}/100 M_{\odot})$, for a duration of 2 Myr each. The accretion rate density is larger in the simulation with HMXBs than in the simulation without HMXBs by up to several orders of magnitude, as expected from the difference in accretion rates of HMXBs and miniquasars.

At the final simulation redshift, the accreted mass densities are still significantly below the CXRB upper limits and hence consistent with observations. However, if BH growth continues down to lower redshifts as expected, the accretion mass densities would likely exceed the CXRB upper limits by $z = 5$. This illustrates the tension between the CXRB limits and models of BH growth that was highlighted by Salvaterra et al. (2012). However, our simulations may overestimate the accretion mass density since a fraction of the Pop III stars may explode in pair instability supernovae instead of col-

lapsing into BHs (e.g., Heger et al. 2003; Chatzopoulos & Wheeler 2012, Yoon et al. 2012), a process that we have ignored. Moreover, at lower redshifts, stellar radiative, kinetic and chemical feedback as well as BH feedback may limit the ability of galaxies to grow BHs, further reducing the accreted mass densities (e.g., Tanaka et al. 2012). The contribution of redshifted radiation from high- z sources to the observed 2–10 keV band depends on their X-ray spectra (see Salvaterra et al. 2012 for a discussion) and will be reduced if the typical spectrum cuts off at rest-frame energies lower than $(40 - 200)/[(1+z)/20]$ keV.

4 IMPACT ON 21 CM SIGNATURE

The 21 cm line of atomic hydrogen is a promising tool to understand the reionization history of the Universe (for reviews see, e.g., Furlanetto et al. 2006; Pritchard & Loeb 2012; Zaroubi 2013). The relevant observable is the differential brightness temperature, i.e., the 21 cm brightness temperature measured against the CMB temperature T_{CMB} , and which in the optically thin limit is given by (e.g., Madau et al. 1997; Furlanetto & Oh 2006)

$$\delta T_{\text{b}} = 40 \text{ mK} (1 + \delta) \eta_{\text{HI}} \left(\frac{1+z}{25} \right)^{1/2} \left(1 - \frac{T_{\text{CMB}}}{T_{\text{s}}} \right), \quad (26)$$

where $\delta \equiv (n_{\text{H}} - \bar{n}_{\text{H}})/\bar{n}_{\text{H}}$ is the density contrast, and T_{s} is the spin temperature. The spin temperature is the weighted sum of the kinetic gas temperature T_{gas} and T_{CMB} ,

$$T_{\text{s}} = \frac{T_{\text{CMB}} + (y_{\text{col}} + y_{\alpha})T_{\text{gas}}}{1 + y_{\text{col}} + y_{\alpha}}, \quad (27)$$

where y_{col} and y_{α} are, respectively, the collisional and Ly α radiative coupling efficiencies (e.g., Wouthuysen 1952; Field 1958), and we have assumed $T_{\text{c}} = T_{\text{gas}}$ for the color temperature T_{c} of the Ly α photons.

Depending on the spin temperature of the hydrogen atom, the 21 cm line may be seen in emission ($\delta T_{\text{b}} > 0$) or absorption ($\delta T_{\text{b}} < 0$). Estimates of the spin temperature are complicated by uncertainties in the radiative coupling by Ly α photons that may originate from stellar atmospheres or from recombining or excited ions, and whose intensity is difficult to compute because it requires solving the RT equation for Ly α photons (e.g., Baek et al. 2009; Yajima & Li 2013). Therefore, most works simply assume either full collisional or full radiative coupling given the circumstances (e.g. Greif et al. 2009; Tokutani et al. 2009). E.g., once the first generation of stars turns on, Ly α coupling is expected to quickly set the spin temperature to the gas temperature (e.g. Chen & Miralda-Escudé 2008; Ciardi et al. 2010; Mesinger et al. 2013). Note from Equation 27 that for $T_{\text{s}} \gg T_{\text{CMB}}$, the differential brightness temperature is independent of the spin temperature (e.g. Scott & Rees 1990).

Here, we compute the 21 cm signal assuming the two limiting cases of pure collisional coupling ($y_{\alpha} = 0$) and perfect coupling to the gas kinetic temperature ($T_{\text{s}} = T_{\text{gas}}$), due to Ly α scattering via the Wouthuysen-Field effect (Wouthuysen 1952; Field 1958), but neglecting any accompanying Ly α heating of the gas. Such a strong radiative coupling is expected after the establishment of a Ly α background by the first stars (e.g., Kuhlen et al. 2006). The efficiency of collisional coupling is given by $y_{\text{col}} = T_{*}(C_{\text{H}} + C_{\text{e}} +$

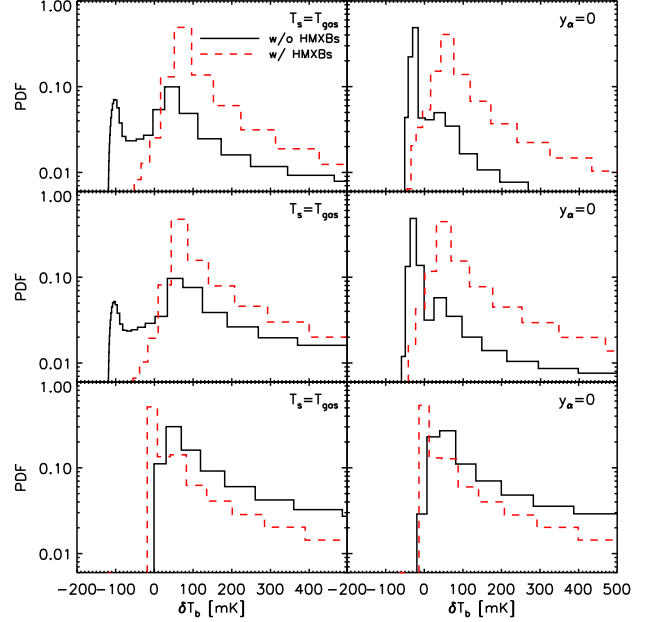


Figure 12. The probability distribution function (PDF) of the differential brightness temperature δT_{b} at $z = 27.8, 25.9,$ and 18.1 (from top to bottom), in the high-resolution regions of the simulations with (red dashed) and without (black solid) HMXBs. Panels in the left column show the PDF computed assuming $T_{\text{s}} = T_{\text{gas}}$, as will be the case after the establishment of a Ly α background by the first ionizing sources, and panels in the right column show the PDF assuming that spin and gas temperatures couple only through collisions ($y_{\alpha} = 0$ in Equation 27).

$C_{\text{p}})/(A_{10}T_{\text{gas}})$. Here, $T_{*} = h\nu_{21 \text{ cm}}/k_{\text{B}} = 0.0681 \text{ K}$ is the temperature associated with the 21 cm hyperfine-structure transition, $A_{10} = 2.85 \times 10^{-15} \text{ s}^{-1}$ is the Einstein A coefficient and $C_{\text{H}}, C_{\text{e}},$ and C_{p} are the de-excitation rates of the triplet state due to collisions with neutral atoms, electrons and protons, respectively. The collisions with neutral atoms are determined by $C_{\text{H}} = n_{\text{H}}\kappa$, where κ is the effective single-atom rate coefficient from Zygelman (2005). The e -H collision term is written as $C_{\text{e}} = n_{\text{e}}\gamma_{\text{e}}$, where γ_{e} is given by Liszt (2001) and Smith (1966). The rate coefficient for proton-induced de-excitation is just 3.2 times larger than that for neutral atoms at $T_{\text{gas}} > 30 \text{ K}$ (Smith 1966), $\gamma_{\text{p}} = 3.2\kappa$, and $C_{\text{p}} = n_{\text{p}}\gamma_{\text{p}}$. Excitation by protons is typically unimportant, as it is much weaker than that by electrons at the same temperature (e.g., Kuhlen et al. 2006).

We point out that our high-resolution region, corresponding to the angular size of $\sim 0.1'$ and a frequency range of $\sim 0.01 \text{ MHz}$ (e.g., Furlanetto et al. 2006), is unlikely to be resolved in observations even with the SKA (e.g., Mellema 2013). However, it is expected that X-ray preionization affects the topology of the 21 cm signal in a similar manner also on much larger scales than investigated here (e.g., Pritchard & Furlanetto 2007; Baek et al. 2010; Mesinger et al. 2013).

Figure 11 shows images of the differential brightness temperature in the high-resolution region and centred on the location of the first stellar binary in the runs with and without HMXBs at three characteristic redshifts $z = 27.8, 25.9,$ and 18.1 , assuming that $T_{\text{s}} = T_{\text{gas}}$. At $z = 27.8$, in both

simulations, the photoheated relic HII region with radius $r \approx 2 - 3$ kpc left behind by the first Pop III binary is characterized by a weak emission signal $0 \text{ mK} \lesssim \delta T_b \lesssim 50 \text{ mK}$. Higher brightness temperatures are achieved in dense neutral pockets and filaments of gas that survived photoevaporation (e.g., Kuhlen et al. 2006). The 21 cm signal outside the relic HII region is very different in the two simulations. In the simulation with HMXBs, X-ray heating induces the gas to glow in emission. In the simulation without HMXBs, on the other hand, the gas remains cold and is observed in absorption. These trends are qualitatively consistent with those in previous works (Chen & Miralda-Escudé 2008; Zaroubi et al. 2007; Thomas & Zaroubi 2008; Tokutani et al. 2009; Venkatesan & Benson 2011; Yajima & Li 2013), and the claim of a prominent 21 cm absorption feature of order $\delta T_b \sim -150 \text{ mK}$ as an observational signature of the first stars (e.g., Cen 2006; Chen & Miralda-Escudé 2008).

Figure 12 compares the probability distribution function of the differential brightness temperature for the two limiting cases of collisional-only and perfect coupling at the three redshifts discussed above. In the simulation with HMXBs, the probability distributions are insensitive to the assumptions made about the spin temperature. At late times, $z = 18.1$, the distributions peak around $\delta T_b = 0$, because of the strong preionization of the gas by HMXBs, confirming the visual impression of Figure 11. In the simulation without HMXBs, on the other hand, the brightness temperature distribution is initially sensitive to the assumptions made about the spin temperature. At $z = 27.8$ and 25.9 , assuming pure collisional coupling implies significantly larger negative peak brightness temperatures ($\delta T_b \sim -50 \text{ mK}$) and hence a weaker 21 cm signal than assuming that the spin temperature equals the gas temperature ($\delta T_b \sim -100 \text{ mK}$). At $z = 18.1$, independent of the assumptions on the spin temperature, the differential brightness temperature distribution peaks near $\delta T_b \sim 50 \text{ mK}$. This contrasts with the location of the peak around $\delta T_b = 0$ in the simulation with HMXBs, and may offer a route to deriving observational constraints on the nature of the high-redshift X-ray sources (e.g., Kuhlen et al. 2006).

Additional constraints on X-ray preionization will come from measurements of the optical depth towards reionization (e.g., Ricotti & Ostriker 2004) and measurements of the kinetic Sunyaev-Zeldovich (kSZ) effect (e.g., Zahn 2012; Mesinger et al. 2013; Park et al. 2013). In combination with observations of high-redshift quasars (e.g., Lidz et al. 2007; Datta et al. 2012), these measurements will help uncovering the properties of the first sources of ionizing radiation and the role of X-rays in the early Universe.

5 SUMMARY AND CONCLUSIONS

High Mass X-ray Binaries (HMXBs) are among the most luminous X-ray sources in the local Universe. Recent high-resolution simulations with realistic cosmological initial conditions have suggested that Pop III stars typically form in binaries or as members of small multiple systems, in departure from the preceding paradigm in which the first stars formed in isolation, thus rendering HMXBs plausible in the high- z Universe as well. Furthermore, the realization that low metallicity favours the formation of HMXBs has led to

an increased interest in the impact of HMXBs on early cosmic history. In this paper, we carried out a set of two radiation hydrodynamic simulations with and without HMXBs to explore the X-ray feedback from black holes accreting diffuse gas and from HMXBs on the surrounding gas, on the larger-scale IGM, on subsequent star formation, and on early reionization.

It is often suggested that X-rays enhance the rate of star formation because additional ionization boosts the abundance of H_2 , thus promoting the cooling of the primordial gas. While our simulation with HMXBs shows such an enhancement in H_2 , we find no strong net effect of X-rays on star formation. The number of haloes with cold gas fraction $\gtrsim 0.1$ is comparable in the simulations with and without HMXBs, and the critical mass for the onset of cooling is insensitive to the presence of HMXBs. Furthermore, the comparison with our preceding work in Jeon et al. (2012) suggests that the impact of HMXBs on star formation is subject to the duty cycle of X-ray emission, such that a longer duty cycle favours a stronger positive feedback.

We should note that we have neglected supernova feedback from Pop III stars, which transfers kinetic energy and propagates metals into the surrounding medium. The metal-enriched medium, capable of forming less massive Population II stars, might experience a rather different feedback history. However, it is a matter of active debate when the transition from Pop III to Pop II star formation occurred and when Pop III star formation terminated. Some studies have suggested that Pop III stars may still form until $z \sim 6$, in regions that are uncontaminated by SN enrichment (e.g. Trenti et al. 2009; Muratov et al. 2013).

Our simulations suggest that ionization by X-ray photons from HMXBs can provide a significant net positive feedback on reionization. The star formation rate is unaffected, but the clumping factor, which parametrizes the recombination rate in the IGM, is reduced by a factor of ~ 2 by the feedback from HMXBs. Such a reduction in the recombination rate makes it easier to keep the reionized gas ionized. We also examine the effect of X-ray feedback on black hole growth and show that the Bondi-Hoyle black hole accretion rates in the presence of HMXBs are significantly reduced. This negative feedback on BH growth could play a role in controlling the abundance of intermediate mass BHs, in the range of $10^4 - 10^5 M_\odot$, in SMBH formation scenarios based on seeds left behind by the first generation of stars (e.g. Tanaka et al. 2012).

Lastly, we compute the differential brightness temperature of the neutral hydrogen 21 cm signal. Our simulations show that a promising way for observing the signature of X-rays in the high- z Universe is through the 21 cm emission signal imprinted by X-ray heating. This signature might depend on the characteristics of the X-ray sources, such as their abundance, luminosity, and effective lifetime. In addition, thanks to the pre-ionization by X-rays, the IGM around X-ray sources can possibly achieve earlier reionization, reflected in the location of the peak of the brightness temperature distribution. Thus, future long-wavelength radio observations offer the exciting prospect for constraining the nature of high-redshift X-ray sources.

ACKNOWLEDGEMENTS

We are grateful to Volker Springel, Joop Schaye, and Claudio Dalla Vecchia for letting us use their versions of GADGET and their data visualization and analysis tools. We further thank Volker Springel for letting us use his implementation of the halo finder FOF as well as his substructure finder SUBFIND. We thank Claudio Dalla Vecchia for his implementation of additional variables in SUBFIND and valuable discussions regarding its use. We thank Ali Rahmati, Milan Raičević, and Joop Schaye for discussions of the radiative transfer code TRAPHIC. We thank Ali Rahmati for commenting on an earlier version of the draft. We thank Craig Booth for discussions of numerical implementations of black hole growth. V. B. and M. J. thank the Max-Planck-Institut für Astrophysik (MPA) for its hospitality during part of the work on this paper. V. B. and M. M. acknowledge support from NSF grant AST-1009928 and NASA ATP grant NNX09AJ33G. A. H. P. receives funding from the European Union's Seventh Framework Programme (FP7/2007-2013) under grant agreement number 301096-proFeSsoR. The simulations were carried out at the Texas Advanced Computing Center (TACC).

REFERENCES

- Abel T., Anninos P., Zhang Y., Norman M. L., 1997, *New Astron.*, 2, 181
- Abel T., Bryan G. L., Norman M. L., 2000, *ApJ*, 540, 39
- Abel T., Norman M. L., Madau P., 1999, *ApJ*, 523, 66
- Abel T., Wise J. H., Bryan G. L., 2007, *ApJL*, 659, L87
- Agarwal B., Khochfar S., Johnson J. L., Neistein E., Dalla Vecchia C., Livio M., 2012, *MNRAS*, 425, 2854
- Ahn K., Iliev I. T., Shapiro P. R., Mellema G., Koda J., Mao Y., 2012, *ApJL*, 756, L16
- Ahn K., Shapiro P. R., 2007, *MNRAS*, 375, 881
- Alvarez M. A., Bromm V., Shapiro P. R., 2006, *ApJ*, 639, 621
- Alvarez M. A., Wise J. H., Abel T., 2009, *ApJL*, 701, L133
- Aykutalp A., Wise J. H., Meijerink R., Spaans M., 2013, *ApJ*, 771, 50
- Baek S., Di Matteo P., Semelin B., Combes F., Revaz Y., 2009, *A&A*, 495, 389
- Baek S., Semelin B., Di Matteo P., Revaz Y., Combes F., 2010, *A&A*, 523, A4
- Barkana R., 2009, *MNRAS*, 397, 1454
- Barkana R., Loeb A., 2001, *Physics Reports*, 349, 125
- Bate M. R., Burkert A., 1997, *MNRAS*, 288, 1060
- Belczynski K., Bulik T., Fryer C. L., 2012, (arXiv:1208.2422)
- Belczynski K., Bulik T., Fryer C. L., Ruitter A., Valsecchi F., Vink J. S., Hurley J. R., 2010, *ApJ*, 714, 1217
- Belczynski K., Bulik T., Heger A., Fryer C., 2007, *ApJ*, 664, 986
- Belczynski K., Bulik T., Rudak B., 2004, *ApJL*, 608, L45
- Bondi H., Hoyle F., 1944, *MNRAS*, 104, 273
- Booth C. M., Schaye J., 2009, *MNRAS*, 398, 53
- Bromm V., 2013, *Rep. Prog. Phys.*, in press (arXiv:1305.5178)
- Bromm V., Coppi P. S., Larson R. B., 2002, *ApJ*, 564, 23
- Bromm V., Kudritzki R. P., Loeb A., 2001, *ApJ*, 552, 464
- Bromm V., Larson R. B., 2004, *ARA&A*, 42, 79
- Bromm V., Loeb A., 2006, *ApJ*, 642, 382
- Cen R., 2006, *ApJ*, 648, 47
- Chatzopoulos E., Wheeler J. C., 2012, *ApJ*, 748, 42
- Chen X., Miralda-Escudé J., 2008, *ApJ*, 684, 18
- Ciardi B., Salvaterra R., Di Matteo T., 2010, *MNRAS*, 401, 2635
- Clark P. C., Glover S. C. O., Klessen R. S., Bromm V., 2011, *ApJ*, 727, 110
- Datta K. K., Friedrich M. M., Mellema G., Iliev I. T., Shapiro P. R., 2012, *MNRAS*, 424, 762
- Di Matteo T., Springel V., Hernquist L., 2005, *Nature*, 433, 604
- Dijkstra M., Gilfanov M., Loeb A., Sunyaev R., 2012, *MNRAS*, 421, 213
- Dijkstra M., Haiman Z., Loeb A., 2004, *ApJ*, 613, 646
- Dijkstra M., Haiman Z., Mesinger A., Wyithe J. S. B., 2008, *MNRAS*, 391, 1961
- Dijkstra M., Haiman Z., Rees M. J., Weinberg D. H., 2004, *ApJ*, 601, 666
- Dopcke G., Glover S. C. O., Clark P. C., Klessen R. S., 2013, *ApJ*, 766, 103
- Dray L. M., 2006, *MNRAS*, 370, 2079
- Edgar R., 2004, *NewAR*, 48, 843
- Efstathiou G., 1992, *MNRAS*, 256, 43P
- Eldridge J. J., Vink J. S., 2006, *A&A*, 452, 295
- Emberson J. D., Thomas R. M., Alvarez M. A., 2013, *ApJ*, 763, 146
- Fan et al. 2006, *AJ*, 131, 1203
- Fialkov A., Barkana R., Visbal E., 2014, *Nature*, 506, 197
- Field G. B., 1958, *Proceedings of the IRE*, 46, 240
- Finlator K., Davé R., Özel F., 2011, *ApJ*, 743, 169
- Finlator K., Oh S. P., Özel F., Davé R., 2012, *MNRAS*, 427, 2464
- Furlanetto S. R., Oh S. P., 2006, *ApJ*, 652, 849
- Furlanetto S. R., Oh S. P., Briggs F. H., 2006, *Physics Reports*, 433, 181
- Furlanetto S. R., Stoever S. J., 2010, *MNRAS*, 404, 1869
- Gilli R., Comastri A., Hasinger G., 2007, *A&A*, 463, 79
- Glover S. C. O., Abel T., 2008, *MNRAS*, 388, 1627
- Glover S. C. O., Brand P. W. J. L., 2003, *MNRAS*, 340, 210
- Gnedin N. Y., 2000, *ApJ*, 542, 535
- Gnedin N. Y., Kravtsov A. V., Chen H.-W., 2008, *ApJ*, 672, 765
- Greif T. H., Bromm V., Clark P. C., Glover S. C. O., Smith R. J., Klessen R. S., Yoshida N., Springel V., 2012, *MNRAS*, 424, 399
- Greif T. H., Glover S. C. O., Bromm V., Klessen R. S., 2010, *ApJ*, 716, 510
- Greif T. H., Johnson J. L., Klessen R. S., Bromm V., 2009, *MNRAS*, 399, 639
- Greif T. H., Springel V., White S. D. M., Glover S. C. O., Clark P. C., Smith R. J., Klessen R. S., Bromm V., 2011, *ApJ*, 737, 75
- Grimm H.-J., Gilfanov M., Sunyaev R., 2003, *MNRAS*, 339, 793
- Haiman Z., 2011, *Nature*, 472, 47
- Haiman Z., Abel T., Madau P., 2001, *ApJ*, 551, 599
- Haiman Z., Abel T., Rees M. J., 2000, *ApJ*, 534, 11
- Haiman Z., Rees M. J., Loeb A., 1997, *ApJ*, 476, 458

- Heger A., Fryer C. L., Woosley S. E., Langer N., Hartmann D. H., 2003, *ApJ*, 591, 288
- Hernquist L., Springel V., 2003, *MNRAS*, 341, 1253
- Hirano S., Hosokawa T., Yoshida N., Umeda H., Omukai K., Chiaki G., Yorke H. W., 2013, *ApJ*, submitted (arXiv:1308.4456)
- Holley-Bockelmann K., Wise J. H., Sinha M., 2012, *ApJL*, 761, L8
- Hosokawa T., Omukai K., Yoshida N., Yorke H. W., 2011, *Science*, 334, 1250
- Jeon M., Pawlik A. H., Greif T. H., Glover S. C. O., Bromm V., Milosavljević M., Klessen R. S., 2012, *ApJ*, 754, 34
- Johnson J. L., Bromm V., 2007, *MNRAS*, 374, 1557
- Johnson J. L., Khochfar S., 2011, *ApJ*, 743, 126
- Johnson J. L., Whalen D. J., Li H., Holz D. E., 2013, *ApJ*, 771, 116
- Justham S., Schawinski K., 2012, *MNRAS*, 423, 1641
- Kato S., Fukue J., Mineshige S., 1998, *Black-hole accretion disks* (Kyoto, University Press)
- Kitayama T., Yoshida N., Susa H., Umemura M., 2004, *ApJ*, 613, 631
- Komatsu E., Smith K. M., Dunkley J., Bennett C. L., Gold B., Hinshaw G., Jarosik N., Larson D., Nolte M. R., Page L., Spergel e. a., 2011, *ApJS*, 192, 18
- Kowalska I., Bulik T., Belczynski K., 2012, *A&A*, 541, A120
- Kroupa P., 2001, *MNRAS*, 322, 231
- Kudritzki R.-P., Puls J., 2000, *ARA&A*, 38, 613
- Kuhlen M., Madau P., 2005, *MNRAS*, 363, 1069
- Kuhlen M., Madau P., Montgomery R., 2006, *ApJL*, 637, L1
- Li Y., 2011, (arXiv:1109.3442)
- Lidz A., McQuinn M., Zaldarriaga M., Hernquist L., Dutta S., 2007, *ApJ*, 670, 39
- Linden T., Kalogera V., Sepinsky J. F., Prestwich A., Zezas A., Gallagher J. S., 2010, *ApJ*, 725, 1984
- Liszt H., 2001, *A&A*, 371, 698
- Loeb A., 2010, *How Did the First Stars and Galaxies Form?* (Princeton University Press, Princeton)
- Machacek M. E., Bryan G. L., Abel T., 2001, *ApJ*, 548, 509
- Machacek M. E., Bryan G. L., Abel T., 2003, *MNRAS*, 338, 273
- Machida M. N., Omukai K., Matsumoto T., Inutsuka S.-i., 2008, *ApJ*, 677, 813
- Madau P., Haardt F., Rees M. J., 1999, *ApJ*, 514, 648
- Madau P., Meiksin A., Rees M. J., 1997, *ApJ*, 475, 429
- Madau P., Rees M. J., Volonteri M., Haardt F., Oh S. P., 2004, *ApJ*, 604, 484
- Majid W. A., Lamb R. C., Macomb D. J., 2004, *ApJ*, 609, 133
- Mapelli M., Colpi M., Zampieri L., 2009, *MNRAS*, 395, L71
- McQuinn M., 2012, *MNRAS*, 426, 1349
- Mellema G. e. a., 2013, *Experimental Astronomy*, 36, 235
- Mellema G., Iliev I. T., Alvarez M. A., Shapiro P. R., 2006, *New Astronomy*, 11, 374
- Mesinger A., Dijkstra M., 2008, *MNRAS*, 390, 1071
- Mesinger A., Ferrara A., Spiegel D. S., 2013, *MNRAS*, 431, 621
- Miller J. M., Fabbiano G., Miller M. C., Fabian A. C., 2003, *ApJL*, 585, L37
- Milosavljević M., Bromm V., Couch S. M., Oh S. P., 2009, *ApJ*, 698, 766
- Milosavljević M., Couch S. M., Bromm V., 2009, *ApJL*, 696, L146
- Mineo S., Gilfanov M., Sunyaev R., 2012, *MNRAS*, 419, 2095
- Mirabel I. F., Dijkstra M., Laurent P., Loeb A., Pritchard J. R., 2011, *A&A*, 528, A149
- Miralda-Escudé J., Haehnelt M., Rees M. J., 2000, *ApJ*, 530, 1
- Mirocha J., Skory S., Burns J. O., Wise J. H., 2012, *ApJ*, 756, 94
- Mitsuda K., Inoue H., Koyama K., Makishima K., Matsuoka M., Ogawara Y., Suzuki K., Tanaka Y., Shibasaki N., Hirano T., 1984, *PASJ*, 36, 741
- Moretti A., Vattakunnel S., Tozzi P., Salvaterra R., Severgnini P., Fugazza D., Haardt F., Gilli R., 2012, *A&A*, 548, A87
- Mortlock D. J., Warren S. J., Venemans B. P., Patel M., Hewett P. C., McMahon R. G., Simpson C., Theuns T., González-Solares E. A., Adamson A., Dye S., Hambly N. C., Hirst P., Irwin M. J., Kuiper E., Lawrence A., Röttgering H. J. A., 2011, *Nature*, 474, 616
- Muratov A. L., Gnedin O. Y., Gnedin N. Y., Zemp M., 2013, *ApJ*, 773, 19
- Oh S. P., 2001, *ApJ*, 553, 499
- Oh S. P., Haiman Z., 2002, *ApJ*, 569, 558
- Okamoto T., Gao L., Theuns T., 2008, *MNRAS*, 390, 920
- O'Shea B. W., Norman M. L., 2008, *ApJ*, 673, 14
- Osterbrock D. E., Ferland G. J., 2006, *Astrophysics of gaseous nebulae and active galactic nuclei* (CA: University Science Books)
- Paardekooper J.-P., Pelupessy F. I., Altay G., Kruij C. J. H., 2011, *A&A*, 530, A87
- Park H., Shapiro P. R., Komatsu E., Iliev I. T., Ahn K., Mellema G., 2013, *ApJ*, 769, 93
- Park K., Ricotti M., 2011, *ApJ*, 739, 2
- Pawlik A. H., Milosavljević M., Bromm V., 2013, *ApJ*, 767, 59
- Pawlik A. H., Schaye J., 2008, *MNRAS*, 389, 651
- Pawlik A. H., Schaye J., 2009, *MNRAS*, 396, L46
- Pawlik A. H., Schaye J., 2011, *MNRAS*, 412, 1943
- Pawlik A. H., Schaye J., van Scherpenzeel E., 2009, *MNRAS*, 394, 1812
- Pelupessy F. I., Di Matteo T., Ciardi B., 2007, *ApJ*, 665, 107
- Petkova M., Springel V., 2011, *MNRAS*, 412, 935
- Planck Collaboration 2013, (arXiv:1303.5076)
- Power C., James G., Combet C., Wynn G., 2013, *ApJ*, 764, 76
- Power C., Wynn G. A., Combet C., Wilkinson M. I., 2009, *MNRAS*, 395, 1146
- Prieto J., Padoan P., Jimenez R., Infante L., 2011, *ApJL*, 731, L38
- Pringle J. E., 1981, *ARA&A*, 19, 137
- Pritchard J. R., Furlanetto S. R., 2007, *MNRAS*, 376, 1680
- Pritchard J. R., Loeb A., 2012, *Reports on Progress in Physics*, 75, 086901
- Razoumov A. O., Sommer-Larsen J., 2006, *ApJL*, 651, L89
- Ricotti M., Gnedin N. Y., Shull J. M., 2001, *ApJ*, 560, 580
- Ricotti M., Gnedin N. Y., Shull J. M., 2002, *ApJ*, 575, 49
- Ricotti M., Ostriker J. P., 2004, *MNRAS*, 352, 547

- Ripamonti E., Mapelli M., Zaroubi S., 2008, MNRAS, 387, 158
- Robertson B. E., Ellis R. S., Dunlop J. S., McLure R. J., Stark D. P., 2010, Nature, 468, 49
- Safraneck-Shrader C., Agarwal M., Federrath C., Dubey A., Milosavljević M., Bromm V., 2012, MNRAS, 426, 1159
- Saigo K., Matsumoto T., Umemura M., 2004, ApJL, 615, L65
- Salvaterra R., Haardt F., Volonteri M., 2007, MNRAS, 374, 761
- Salvaterra R., Haardt F., Volonteri M., Moretti A., 2012, A&A, 545, L6
- Sazonov S. Y., Ostriker J. P., Sunyaev R. A., 2004, MNRAS, 347, 144
- Schaerer D., 2003, A&A, 397, 527
- Schaye J., 2001a, ApJL, 562, L95
- Schaye J., 2001b, ApJ, 559, 507
- Schaye J., Dalla Vecchia C., Booth C. M., Wiersma R. P. C., Theuns T., Haas M. R., Bertone S., Duffy A. R., McCarthy I. G., van de Voort F., 2010, MNRAS, 402, 1536
- Scott D., Rees M. J., 1990, MNRAS, 247, 510
- Shakura N. I., Sunyaev R. A., 1973, A&A, 24, 337
- Shapiro P. R., Giroux M. L., Babul A., 1994, ApJ, 427, 25
- Shu F. H., Lizano S., Galli D., Cantó J., Laughlin G., 2002, ApJ, 580, 969
- Shull J. M., Harness A., Trenti M., Smith B. D., 2012, ApJ, 747, 100
- Shull J. M., van Steenberg M. E., 1985, ApJ, 298, 268
- Sijacki D., Springel V., Di Matteo T., Hernquist L., 2007, MNRAS, 380, 877
- Smith F. J., 1966, Planetary Space Sci., 14, 929
- Smith R. J., Glover S. C. O., Clark P. C., Greif T., Klessen R. S., 2011, MNRAS, 414, 3633
- Sobacchi E., Mesinger A., 2013, MNRAS, 432, 3340
- Soria R., 2007, Ap&SS, 311, 213
- Springel V., 2005, MNRAS, 364, 1105
- Springel V., Di Matteo T., Hernquist L., 2005, MNRAS, 361, 776
- Springel V., Hernquist L., 2002, MNRAS, 333, 649
- Springel V., White S. D. M., Tormen G., Kauffmann G., 2001, MNRAS, 328, 726
- Stacy A., Bromm V., 2013, MNRAS, 433, 1094
- Stacy A., Greif T. H., Bromm V., 2010, MNRAS, 403, 45
- Stacy A., Greif T. H., Bromm V., 2012, MNRAS, 422, 290
- Tanaka T., Perna R., Haiman Z., 2012, MNRAS, 425, 2974
- Tegmark M., Silk J., Rees M. J., Blanchard A., Abel T., Palla F., 1997, ApJ, 474, 1
- Thomas R. M., Zaroubi S., 2008, MNRAS, 384, 1080
- Thoul A. A., Weinberg D. H., 1996, ApJ, 465, 608
- Tokutani M., Yoshida N., Oh S. P., Sugiyama N., 2009, MNRAS, 395, 777
- Treister E., Schawinski K., Volonteri M., Natarajan P., Gawiser E., 2011, Nature, 474, 356
- Trenti M., Stiavelli M., Michael Shull J., 2009, ApJ, 700, 1672
- Turk M. J., Abel T., O’Shea B., 2009, Science, 325, 601
- Venkatesan A., Benson A., 2011, MNRAS, 417, 2264
- Verner D. A., Ferland G. J., Korista K. T., Yakovlev D. G., 1996, ApJ, 465, 487
- Volonteri M., Bellovary J., 2012, Reports on Progress in Physics, 75, 124901
- Volonteri M., Gnedin N. Y., 2009, ApJ, 703, 2113
- Whalen D., Abel T., Norman M. L., 2004, ApJ, 610, 14
- Wheeler J. C., Johnson V., 2011, ApJ, 738, 163
- Wiklind T., Mobasher B., Bromm V., eds, 2013, The First Galaxies Vol. 396 of Astrophysics and Space Science Library
- Willott C. J., Delorme P., Reylé C., Albert L., Bergeron J., Crampton D., Delfosse X., Forveille T., Hutchings J. B., McLure R. J., Omont A., Schade D., 2010, AJ, 139, 906
- Wise J. H., Abel T., 2005, ApJ, 629, 615
- Wise J. H., Abel T., 2008a, ApJ, 684, 1
- Wise J. H., Abel T., 2008b, ApJ, 685, 40
- Wise J. H., Cen R., 2009, ApJ, 693, 984
- Wise J. H., Turk M. J., Norman M. L., Abel T., 2012, ApJ, 745, 50
- Wolcott-Green J., Haiman Z., 2011, MNRAS, 412, 2603
- Wolcott-Green J., Haiman Z., Bryan G. L., 2011, MNRAS, 418, 838
- Wouthuysen S. A., 1952, AJ, 57, 31
- Xu H., Wise J. H., Norman M. L., 2013, ApJ, 773, 83
- Yajima H., Choi J.-H., Nagamine K., 2011, MNRAS, 412, 411
- Yajima H., Li Y., 2013, (arXiv:1308.0381)
- Yoon S.-C., Dierks A., Langer N., 2012, A&A, 542, A113
- Yoshida N., Abel T., Hernquist L., Sugiyama N., 2003, ApJ, 592, 645
- Yoshida N., Oh S. P., Kitayama T., Hernquist L., 2007, ApJ, 663, 687
- Zahn O. e. a., 2012, ApJ, 756, 65
- Zaroubi S., 2013, in Wiklind T., Mobasher B., Bromm V., eds, Astrophysics and Space Science Library Vol. 396 of Astrophysics and Space Science Library, The Epoch of Reionization. p. 45
- Zaroubi S., Thomas R. M., Sugiyama N., Silk J., 2007, MNRAS, 375, 1269
- Zygelman B., 2005, ApJ, 622, 1356